CHAPTER 11

Computational investigation on the Physio-chemical, Structural and Binding features of BA.2.75 and BA.2.75.2 Omicron variants of SARS-CoV-2

Computational investigation on the Physio-chemical, Structural and Binding features of BA.2.75 and BA.2.75.2 Omicron variants of SARS-CoV-2

11.1. Abstract:

Recently, several Omicron sub lineages, including BA.2, BA.4, and BA.5 have demonstrated even better immune evasion and are responsible for waves of infections across the globe. BA.2.75, an Omicron sub lineage, had been found in at least 15 nations and has become more prevalent in India. Additionally, a sub-lineage of BA.2.75 (BA.2.75.2) that has recently emerged and expanded quickly and it carries additional mutations R346T, F486S, and D1199N suggested a more extensive escape from neutralizing antibodies. In this study, physiochemical and structural characteristics of the spike protein of BA.2.75 and BA.2.75.2 variants were analyzed by employing various online tools and MD simulation and other computational approaches. The spike proteins of these variants were found to have higher aliphatic index indicating their stability across a wide range of temperatures. About 6.61% of the region of spike protein was found to be disordered in BA.2.75 and BA.2.75.2. The mutations G446S, R493Q, Q498R, N501Y and N505H present in the RBD region of spike protein of BA.2.75 and BA.2.75.2 were found to play a significant role in the binding of RBD of spike to the ACE2. From the RMSD, RMSF, and number of inter-molecular hydrogen bond analyses, we found the Spike protein (BA.2.75)-ACE2 complex to have enhanced stability than the Spike protein (BA.2.75.2)-ACE2 complex. Also, we found the binding free energy value for the Spike (BA.2.75)-ACE2 complex (GB_{TOT}= -20.03 kcal/mol) to be relatively higher than the Spike (BA.2.75.2)-ACE2 complex (GB_{TOT}= -15.19 kcal/mol). The overall stability of the Spike protein (BA.2.75)-ACE2 complex and the increased affinity between spike protein (BA.2.75) and ACE2 may result in higher virulence of the strain.

11.2. Introduction:

The ongoing spread of an infectious Coronavirus disease 2019 (COVID-19), caused by severe acute respiratory syndrome-Coronavirus-2 (SARS-CoV-2), an enveloped positive-stranded RNA virus in the community, poses exceptional challenges for the healthcare system due to high incidence and long incubation time [1]. Since the start of 2022, the majority of worldwide outbreaks have been caused by the coronavirus Omicron variants, which are constantly evolving. The Omicron variants raise worries that it could be associated with higher transmissibility, decreased vaccination effectiveness, and a higher risk of reinfection [2,3]. Omicron's sub-variants BA.4 and BA.5 were discovered to be common in Europe and America, but a new sub-lineage, BA.2.75, has been discovered in India in May 2022

and was found to drive a wave of infections in India, and has spread internationally [4]. Omicron sub-variant BA.2.75, even though not much study is still being not done on it, is more transmissible, according to WHO. Health professionals state that even though BA.2.75 is a fast-spreading variant with numerous spike mutations developing simultaneously, it is still too soon to determine with certainty just how much better BA.2.75 is at evading vaccine-induced and innate immunity. Additionally, BA.2.75 has a regional better adaptation over BA.2.38 and BA.4/BA.5. Its immune evasion capability and receptor binding affinity is unclear and requires investigation [5,6]. Relative to BA.2, BA.2.75 carries three additional mutations in the RBD of spike protein: G339H, G446S and N460K [7] with a total of 17 mutations on its RBD. And a sub lineage of BA.2.75 (BA.2.75.2) harboring the additional mutations R346T, F486S, and D1199N emerged, expanding quickly, and suggesting a wider escape from neutralizing antibodies [2]. The pathogenicity of the BA.2.75 sub-variant is attributed to the presence of two distinct mutations. The first is G446S, a location that contributes significantly to this variant's resistance to antibodies generated by existing vaccinations [8]. The second mutation is R493Q, which permits the virus to connect to ACE2 receptors, allowing it to adhere to cells more easily [9]. Preliminary investigations suggest that BA.2.75 is more transmissible than the other BA.2 sub-variants [10]. The additional mutations (R346T and F486S) present in the BA.2.75.2 were found to contribute enhanced resistance of BA.2.75.2 compared with BA.2.75 [2].

The omicron symptoms are more similar to those of the common cold, such as runny nose, sneezing, and sore throat, as compared to the usual symptoms of cough, cold, fever, and loss of taste and smell [11]. Some studies indicate that vaccinated individuals experience milder omicron symptoms than non-vaccinated individuals [11]. Since BA.2.75 and its sublineage BA.2.75.2 have emerged recently, there isn't a lot of information accessible. BA.2.75 and its sublineage BA.2.75.2 are considered to be more transmissible than other variants and have the ability to overcome the immunity built up from prior infections or vaccinations. However, it is still too early to draw any conclusions about the course of action [12-19]. Only a few studies have been carried out to check whether the omicron BA.2.75 and its sublineage BA.2.75.2 to develop a more severe infection than its predecessor's corona variants and to combat those emerging SARS-CoV-2 strains, new vaccinations may need to be developed regularly [20-27]. With the introduction of extremely infectious SARS-CoV-2 variants, greater vaccine penetration will be required to build protective immunity [28-33]. In this study, we have employed computational techniques to evaluate the physiochemical and structural characteristics of the spike protein of BA.2.75 and its sub-lineage BA.2.75.2.

11.3. Materials and Methods:

11.3.1. Data retrieval

The FASTA sequence of the BA.2.75 SARS-CoV-2 spike protein (S protein) was obtained from NCBI (GenBank Id: UTM82166.1). The FASTA sequence for BA.2.75.2 was obtained by the addition of three mutations (R346T, F486S, and D1199N) in the FASTA sequence of BA.2.75.

11.3.2. Analysis of physicochemical parameter

The ExPASy ProtParam [34] online tool was used to examine the physio-chemical properties of S protein of BA.2.75 and BA.2.75.2 Omicron variants from their sequence. The molecular weight, pI, amino acid composition, atomic composition, extinction coefficient, projected half-life, instability index, aliphatic index, and overall hydropathicity were all calculated using ProtParam tool.

11.3.3. Prediction of secondary structural changes in spike protein

The secondary structure information regarding the S protein of BA.2.75 and BA.2.75.2 variants of SARS-CoV-2 were obtained using GOR IV [35]. Information theory and Bayesian statistics are generally used by the Garnier-Osguthorpe-Robson (GOR) tool to examine the secondary structure of the protein. GOR is used to combine several sequence alignments in order to learn more about how to better differentiate secondary structures.

11.3.4. Identification of conserved residues

Clustal Omega [36] a bioinformatics program, was used to identify the conserved residues by aligning the Wuhan-Hu-1 (wild-type) S protein amino acid sequence with the amino acid sequence of Omicron variants BA.2.75 and BA.2.75.2.

11.3.5. Intrinsically disordered protein prediction

Regions with intrinsic disorder are those that have a dynamic ensemble of conformations but do not develop a stable three-dimensional structure in physiological situations. Using the Predictor of naturally disordered regions (PONDR) (PONDR® VLXT) [37], the disordered regions in the S protein of Wuhan Hu-1, BA.2.75 and BA.2.75.2 variants were determined.

11.3.6. Prediction of protein stability

The effect of single point mutation on the stability of the S protein of BA.2.75 and BA.2.75.2 variants were predicted using I-Mutant 3.0 [38]. It is a support vector machine-based tool for predicting protein stability changes resulting from single point mutations. It may be used to predict the sign of the protein stability change caused by mutation, as well as a regression estimator to predict the associated G values. Protein structure dynamics and flexibility are also important aspects of protein function.

11.3.7. Protein-Protein interaction of the RBD of Spike protein (BA.2.75/BA.2.75.2)-ACE2 complexes

The Research Collaboratory for Structural Bioinformatics Protein Data bank (www.rcsb.org) was used to obtain the initial 3-D structure of the SARS-CoV-2 spike receptor-binding domain bound with ACE2 (S protein (WT)-ACE2) (PDB ID: 6lzg with a resolution of 2.50 Å) [39]. The RBD of the S protein and the ACE2 were segregated from the 6lzg complex using the UCSF Chimera package alpha v.1.12 [40], and punctual mutations were introduced into the RBD of the S protein to obtain the RBD for BA.2.75 and BA.2.75.2 sublineage (shown in **Figure 11.1A and 11.C**). Then, using Patchdock and Firedock online docking servers, the S protein (BA.2.75)-ACE2 and S protein (BA.2.75.2)-ACE2 complex structures (shown in **Figure 11.1B and 11.1D**) were obtained by submitting the corresponding mutated RBD of S protein and ACE2 to the online docking servers. To get the protein-protein interactions, the docked complex structures were then submitted to the PDBsum server [41].

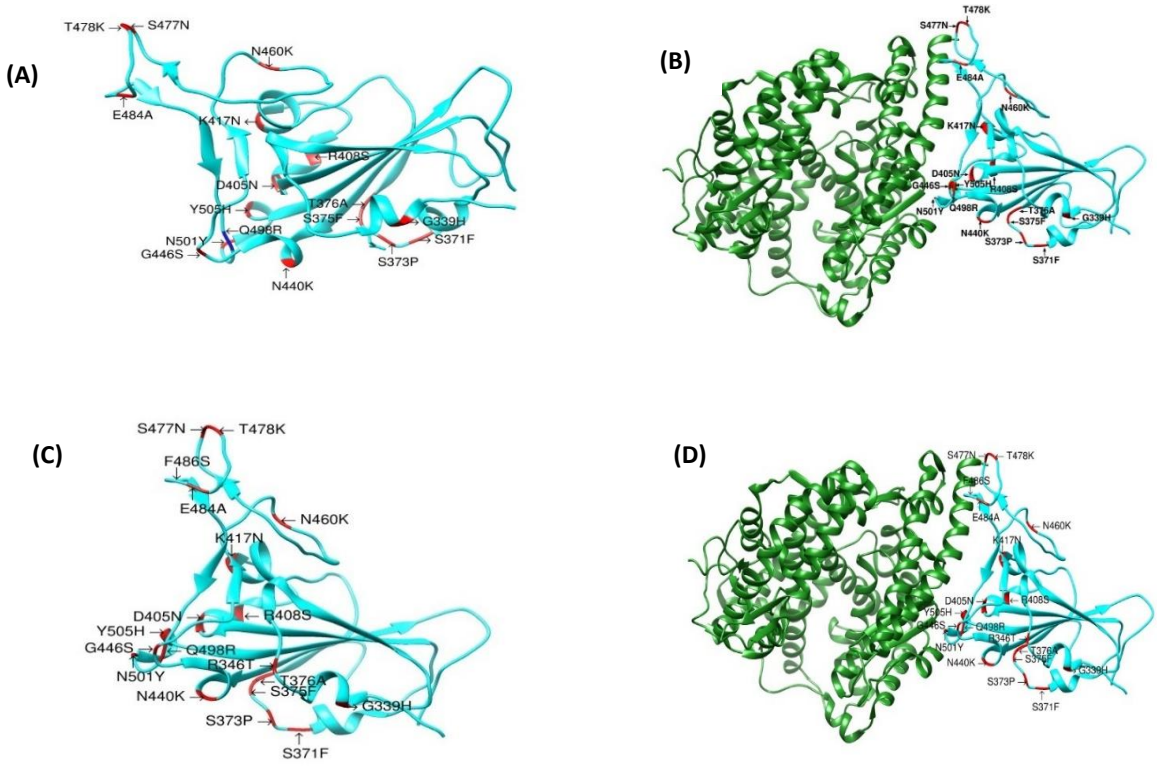

***Figure 11.1**. **(A)** BA.2.75 variant mutations in receptor-binding domain (RBD)of Spike protein. **(B)** BA.2.75 variant mutations in receptor-binding domain of spike protein bound with the ACE2 receptor. **(C)** BA.2.75.2 variant mutations in receptor-binding domain (RBD) of spike protein **(D)** BA.2.75.2 variant mutations in receptor-binding domain of spike protein bound with the ACE2 receptor. The mutations are also labeled.*

11.3.8. Effect of mutations on Protein functioning

Based on sequence homology and the physical characteristics of amino acids, SIFT predicts whether a particular mutation will impact protein function. Both naturally occurring nonsynonymous polymorphisms and missense mutations created in the lab can be analyzed using SIFT. The effect of single point mutation on the S protein functioning in BA.2.75 and BA.2.75.2 variants were predicted using SIFT [42]. The effect in the protein functioning for all the 33 mutations present in the S protein of BA.2.75 and 36 mutations in BA.2.75.2 were analyzed based on its tolerance/intolerance score.

11.3.9. Molecular Dynamics (MD) simulations.

Both the complex of SARS-CoV-2 spike receptor-binding domain bound with ACE2, was subjected to MD simulations. The MD simulation was performed using AMBER ff14SB force field with AMBER software package [43,44]. To ensure the overall neutrality of the two complex systems, appropriate numbers of counter ions were added. MD simulations in an explicit solvent were performed on the two complex systems and were solvated in all directions with a TIP3P [45,46] water model with a solvent buffer of 10 Å. In the first step of minimization, spike receptor-binding domain and ACE2 were fixed with a 500 kcal/mol/Å^2. They minimized the energy of all water molecules and counter ions for 10000 steps of steepest descents (SD) followed by 10000 steps of the conjugate gradient (CG). Subsequently, in the second step of minimization, to remove conflicting contacts, the entire complex system was repeated for 12000 steps of SD minimization and 8000 steps of CG minimization. Next, the complex system in constant volume conditions was heated up gradually from 0-300K, thereby applying harmonic restraints with force constant of 10 kcal/mol/Å^2 on the solute atoms, and equilibration was performed three times with 3000 ps using a force constant of 5.0 kcal/mol/Å^2. Finally, 100 ns MD simulations were performed using the NPT ensemble without restraints. With the non-bonded cutoff of 12.0 Å, we applied the particle mesh Ewald [47,48] approach of 12.0 Å to limit the direct space sum to treat the long-range electrostatic interactions. The SHAKE algorithm [49] was used to limit all the bonds in the system. The Berendsen weak coupling method [50] was used throughout the simulation to keep the pressure and temperature constant (0.5 ps of heat bath and 0.2 ps of pressure relaxation). The time step of MD simulation was set to 2 fs, and sampling was performed every 10 ps into the MD file.

11.3.10. Binding free energy calculations.

The Molecular Mechanics Generalized Born Surface Area (MM-GBSA) method implemented in AMBER 16 [51] package was performed to calculate the binding free energy as well as the free energy decomposition of the two complex systems (S protein (BA.2.75)-ACE2 and S protein (BA.2.75.2)-ACE2).

The formulas for calculating the BFE and their decomposed energetic components are same as described in section 7A.3.2 of Chapter 7A. Many recent in-silico investigations have employed the methodologies and protocols that we explored in this study to estimate the binding free energy [52-54] and a similar protocol was employed in our earlier studies on SARS-CoV-2 variants [55-58].

11.4. Results and Discussion:

11.4.1. Determination of physical parameters of the proteins

Omicron variants (BA.2.75 and BA.2.75.2) having 1270 amino acids, compared to Wuhan Hu1's 1273, however due to sequence loss, they have a few fewer residues than the wild-type. The pH level at which a specific molecule (protein) has no net electrical charge is known as the isoelectric point (pI). The pH of the molecule's environment has an impact on its net charge, which can shift more positively or negatively depending on whether protons are added or taken away. The protein is said to be alkaline if its pI value is greater than 7, and acidic if it is lower than 7. With a theoretical pI of 7.17 (alkaline), the molecular weights of the variants BA.2.75 and BA.2.75.2 are calculated to be 141176.77 and 141060.60, respectively. A number of 40 or above denotes structural instability of the protein. The instability index value for the BA.2.75 and BA.2.75.2 Omicron variants was determined to be 34.26. From this observation, we can infer that these proteins to be stable. These omicron variations had an average extinction value of 146440 M^{-1} cm^{-1}, which represents the amount of light the protein can absorb at 280 nm. The volume of a protein that is occupied by aliphatic amino acids on the side chain, such alanine, is measured by the aliphatic index. Both of these omicron variants were observed to have a high aliphatic index value of 84.95. As a result, these proteins can withstand a wide variety of temperatures and thus they are more thermostable. The degree to which amino acids in a protein sequence are hydrophobic or hydrophilic is referred to as hydropathicity. A protein with a low grand average of hydropathicity (GRAVY) value is nonpolar and has a stronger affinity for water, indicating that it is intrinsically hydrophilic. The GRAVY value was found to be -0.076 for both BA.2.75 and BA.2.75.2 variants. The amino acids arginine (Arg, 3.4%), lysine (Lys, 5.1%), aspartic acid (Asp, 4.7%), and glutamic acid (Glu, 3.8%) dominate in the composition of the BA.2.75 and BA.2.75.2

Omicron variants, indicating that these variants have more charged residues that contribute to salt bridge formation and that charged residues are exposed to a much greater degree. Further these variants also found to contain higher composition of hydrophobic amino acids: phenylalanine (Phe, 6.1%), isoleucine (Ile, 6.0%). These hydrophobic amino acids were observed to be positioned inside the protein core. The RBD of the S protein of these variants were found to contain higher composition of nonpolar amino acids such as leucine (Leu, 6.7%), phenylalanine (Phe, 8.2%) and proline (Pro, 5.7%). These residues are located inside the protein core and are thus inaccessible to the solvent.

11.4.2. Mutations on the BA.2.75 and BA.2.75.2 spike protein

Relative to BA.2, BA.2.75 carries three additional mutations in the RBD of S protein: G339H, G446S and N460K with a total of 17 mutations on its RBD with a total of 34 mutations on the whole spike protein of the SARS-CoV-2. On the other hand, BA.2.75.2 carries 2 additional mutations in the RBD and overall, three additional mutations compared to BA.2.75 as shown in **Table 11.1.**

Table 11.1. *Spike protein mutation in BA.2.75 and BA.2.75.2 variant compared to wild-type (Wuhan-Hu-1)*

Variant	Mutation
Wuhan-Hu-1 (wild-type)	-
Omicron BA.2.75	T19I, LPPA24-7S, G142D, K147E, W152R, F157L, I210V, V213G, G257S, **G339H, S371F, S373P, S375F, T376A, D405N, R408S, K417N, N440K, G446S, N460K, S477N, T478K, E484A, Q498R, N501Y, Y505H,** D614G, H655Y, N679K, P681H, N764K, D796Y, Q954H, N969K
Omicron BA.2.75.2	T19I, LPPA24-7S, G142D, K147E, W152R, F157L, I210V, V213G, G257S, **G339H, R346T, S371F, S373P, S375F, T376A, D405N, R408S, K417N, N440K, G446S, N460K, S477N, T478K, E484A, F486S, Q498R, N501Y, Y505H,** D614G, H655Y, N679K, P681H, N764K, D796Y, Q954H, N969K, D1199N

11.4.3. Prediction of secondary structural changes

GOR IV was used to predict the secondary structure of the BA.2.75 and BA.2.75.2 variant of SARS-CoV-2 and the results shows that the highest percentage was contributed by the alpha helix followed by extended strand and random coil as shown in **Table 11.2**.

Table 11.2. *Secondary structure analysis for BA.2.75 and BA.2.75.2 variant*

Types of secondary structure	**BA.2.75 Omicron variant Entire Protein Percentage (%)**	**BA.2.75 Omicron variant of RBD Percentage (%)**	**BA.2.75.2 Omicron variant Entire Protein Percentage (%)**	**BA.2.75.2 Omicron variant of RBD Percentage (%)**
Alpha helix (Hh)	23.78	9.79	23.23%	9.09%
310 helix (Gg)	0.00	0.00	0.00%	0.00%
Pi helix (Ii)	0.00	0.00	0.00%	0.00%
Beta bridge (Bb)	0.00	0.00	0.00%	0.00%
Extended strand (Ee)	20.31	18.04	21.02%	18.66%
Beta turn (Tt)	0.00	0.00	0.00%	0.00%
Bend region (Ss)	0.00	0.00	0.00%	0.00%
Random coil (Cc)	55.91	72.16	55.75%	72.25%
Ambiguous states	0.00	0.00	0.00%	0.00%
Other states	0.00	0.00	0.00%	0.00%

11.4.4. Identification of conserved residues and mutation

Clustal Omega a bioinformatics program, was used to align the Wuhan-Hu-1 (wild-type) sequence with variant of BA.2.75 and BA.2.75.2 sequences. Clustal Omega is a new multiple sequence alignment program that uses seeded guide trees and HMM profile-profile techniques to generate alignments between **three or more** sequences. The identity and similarity percentage observed between Wild type and the Omicron variants from the sequence alignment have been shown in the **Table 11.3**. BA.2.75 and BA.2.75.2 sequences showed a significantly higher percentage of identity (similarity) in their sequence.

Table 11.3. *The Identity and similarity percentage in the amino acid sequence for Wild type (WT) and Omicron variants (BA.2.75 and BA.2.75.2).*

	WT and BA.2.75	WT and BA.2.75.2	BA.2.75 and BA.2.75.2
Identity	97.1%	96.9%	99.8%
Similarity	98.6%	98.4%	99.8%

11.4.5 Intrinsically disordered prediction

PONDR® VLXT determine the number of ordered and disordered regions and specifically provide us with the regions that are ordered and regions that are disordered in any protein. **Figure 7D.2A and 7D.2B** depicts the PONDR score as a function of residue number for BA.2.75 and BA.2.75.2 Omicron variants. The details regarding the number of disordered residues, overall percent disordered, disordered segments along with their average strength and number of disordered regions in BA.2.75

and BA.2.75.2 have been tabulated in the **Table 7D.4 and 7D.5** respectively. Nearly 6.61% of entire S protein and about 1.03% of RBD of S protein were found to be disordered in BA.2.75 and BA.2.75.2.

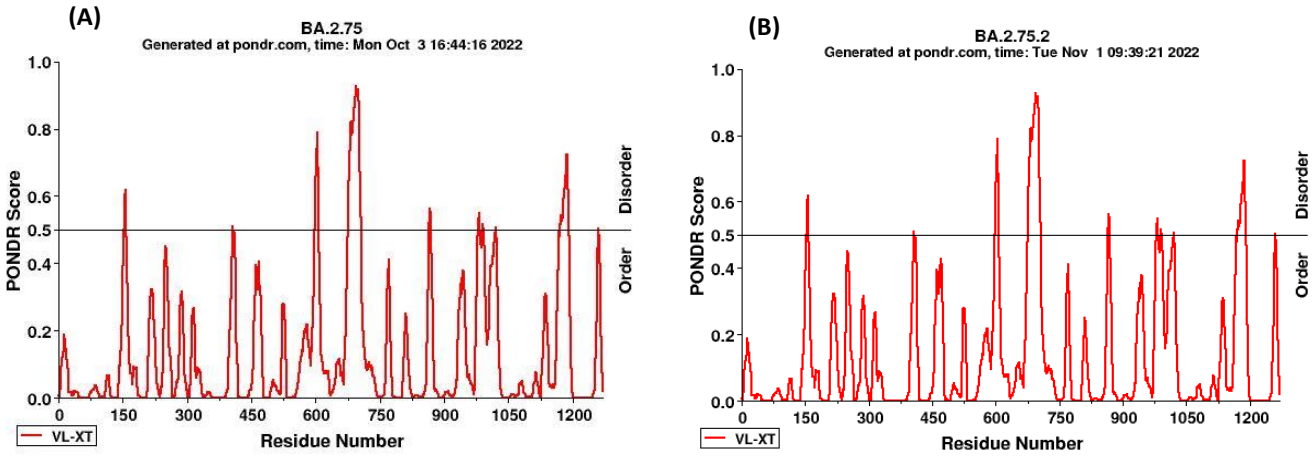

Figure 11.2. *PONDR score as a function of residue number analyzed for* ***(A)*** *BA.2.75 and* ***(B)*** *BA.2.75.2 using PONDR® VLXT*

Table 11.4. *Intrinsically disordered prediction for BA.2.75 variant using PONDR® VLXT*

	No. of residues disordered	Overall percent disordered	Predicted disordered segment	Average strength	Number of disordered regions
Omicron BA.2.75	84	6.61	[153]-[158]	0.5678	10
			[406]-[407]	0.5085	
			[598]-[607]	0.6681	
			[675]-[706]	0.7836	
			[866]-[868]	0.5518	
			[979]-[983]	0.5227	
			[989]-[991]	0.5143	
			[1020]-[1020]	0.5047	
			[1171]-[1191]	0.6043	
			[1261]-[1261]	0.5035	
Omicron RBD BA.2.75	2	1.03	[406]-[407]	0.5085	1

Table 11.5. *Intrinsically disordered prediction for BA.2.75.2 variant using PONDR® VLXT*

	No. of residues disordered	Overall percent disordered	Predicted disordered segment	Average strength	Number of disordered regions
Omicron BA.2.75.2	84	6.61	[153]-[158]	0.5678	10
			[406]-[407]	0.5085	
			[598]-[607]	0.6681	
			[675]-[706]	0.7836	
			[866]-[868]	0.5518	
			[979]-[983]	0.5227	
			[989]-[991]	0.5143	

			[1020]-[1020]	0.5047	
			[1171]-[1191]	0.6043	
			[1261]-[1261]	0.5035	
Omicron RBD BA.2.75.2	2	1.03	[406]-[407]	0.5085	1

The ordered and disordered regions present in the whole spike and RBD of BA.2.75 variant as a function of amino acid sequence is depicted in the **Figure 7D.3 and 7D.4** respectively. The ordered and disordered regions present in the whole spike and RBD of BA.2.75.2 variant as a function of amino acid sequence are depicted in the **Figure 7D.5 and 7D.6** respectively.

```
1        MFVFLVLLPL VSSQCVNLIT RTQSYTNSFT RGVYYPDKVF RSSVLHSTQD
VLXT

51       LFLPFFSNVT WFHAIHVSGT NGTKRFDNPV LPFNDGVYFA STEKSNIIRG
VLXT

101      WIFGTTLDSK TQSLLIVNNA TNVVIKVCEF QFCNDPFLDV YYHENNKSRM
VLXT

151      ESELRVYSSA NNCTFEYVSQ PFLMDLEGKQ GNFKNLREFV FKNIDGYFKI
VLXT       DDDDDD

201      YSKHTPVNLG RDLPQGFSAL EPLVDLPIGI NITRFQTLLA LHRSYLTPGD
VLXT

251      SSSSWTAGAA AYYVGYLQPR TFLLKYNENG TITDAVDCAL DPLSETKCTL
VLXT


301      KSFTVEKGIY QTSNFRVQPT ESIVRFPNIT NLCPFHEVFN ATRFASVYAW
VLXT

351      NRKRISNCVA DYSVLYNFAP FFAFKCYGVS PTKLNDLCFT NVYADSFVIR
VLXT

401      GNEVSQIAPG QTGNIADYNY KLPDDFTGCV IAWNSNKLDS KVSGNYNYLY
VLXT           DD

451      RLFRKSKLKP FERDISTEIY QAGNKPCNGV AGFNCYFPLQ SYGFRPTYGV
VLXT

501      GHQPYRVVVL SFELLHAPAT VCGPKKSTNL VKNKCVNFNF NGLTGTGVLT
VLXT

551      ESNKKFLPFQ QFGRDIADTT DAVRDPQTLE ILDITPCSFG GVSVITPGTN
VLXT                                                       DDD

601      TSNQVAVLYQ GVNCTEVPVA IHADQLTPTW RVYSTGSNVF QTRAGCLIGA
VLXT     DDDDDDD

651      EYVNNSYECD IPIGAGICAS YQTQTKSHRR ARSVASQSII AYTMSLGAEN
VLXT                               DDDDDD DDDDDDDDDD DDDDDDDDDD
```

```
701       SVAYSNNSIA IPTNFTISVT TEILPVSMTK TSVDCTMYIC GDSTECSNLL
VLXT      DDDDDD

751       LQYGSFCTQL KRALTGIAVE QDKNTQEVFA QVKQIYKTPP IKYFGGFNFS
VLXT

801       QILPDPSKPS KRSFIEDLLF NKVTLADAGF IKQYGDCLGD IAARDLICAQ
VLXT

851       KFNGLTVLPP LLTDEMIAQY TSALLAGTIT SGWTFGAGAA LQIPFAMQMA
VLXT                    DDD

901       YRFNGIGVTQ NVLYENQKLI ANQFNSAIGK IQDSLSSTAS ALGKLQDVVN
VLXT

951       HNAQALNTLV KQLSSKFGAI SSVLNDILSR LDKVEAEVQI DRLITGRLQS
VLXT                                  DD DDD     DD D

1001      LQTYVTQQLI RAAEIRASAN LAATKMSECV LGQSKRVDFC GKGYHLMSFP
VLXT                         D

1051      QSAPHGVVFL HVTYVPAQEK NFTTAPAICH DGKAHFPREG VFVSNGTHWF
VLXT

1101      VTQRNFYEPQ IITTDNTFVS GNCDVVIGIV NNTVYDPLQP ELDSFKEELD
VLXT

1151      KYFKNHTSPD VDLGDISGIN ASVVNIQKEI DRLNEVAKNL NESLIDLQEL
VLXT                           DDDDDDDDDD DDDDDDDDDD D

1201      GKYEQYIKWP WYIWLGFIAG LIAIVMVTIM LCCMTSCCSC LKGCCSCGSC
VLXT

1251      CKFDEDDSEP VLKGVKLHYT
VLXT                D
```

Figure 11.3: *Intrinsically disordered prediction for the complete sequence of spike protein of BA.2.75 variant showing the ordered regions represented by " " and disordered regions represented by "D", analyzed using PONDR® VLXT*

```
333       TNLCPFHEVF NATRFASVYA WNRKRISNCV ADYSVLYNFA PFFAFKCYGV
VLXT

383       SPTKLNDLCF TNVYADSFVI RGNEVSQIAP GQTGNIADYN YKLPDDFTGC
VLXT                                  DD

433       VIAWNSNKLD SKVSGNYNYL YRLFRKSKLK PFERDISTEI YQAGNKPCNG
VLXT

483       VAGFNCYFPL QSYGFRPTYG VGHQPYRVVV LSFELLHAPA TVCG
VLXT
```

Figure 11.4: *Intrinsically disordered prediction for the sequence of RBD of spike protein for BA.2.75 variant showing the ordered regions represented by " " and disordered regions represented by "D", analyzed using PONDR® VLXT*

```
1        MFVFLVLLPL VSSQCVNLIT RTQSYTNSFT RGVYYPDKVF RSSVLHSTQD
VLXT

51       LFLPFFSNVT WFHAIHVSGT NGTKRFDNPV LPFNDGVYFA STEKSNIIRG
VLXT

101      WIFGTTLDSK TQSLLIVNNA TNVVIKVCEF QFCNDPFLDV YYHENNKSRM
VLXT

151      ESELRVYSSA NNCTFEYVSQ PFLMDLEGKQ GNFKNLREFV FKNIDGYFKI
VLXT       DDDDDD

201      YSKHTPVNLG RDLPQGFSAL EPLVDLPIGI NITRFQTLLA LHRSYLTPGD
VLXT

251      SSSSWTAGAA AYYVGYLQPR TFLLKYNENG TITDAVDCAL DPLSETKCTL
VLXT

301      KSFTVEKGIY QTSNFRVQPT ESIVRFPNIT NLCPFHEVFN ATTFASVYAW
VLXT

351      NRKRISNCVA DYSVLYNFAP FFAFKCYGVS PTKLNDLCFT NVYADSFVIR
VLXT

401      GNEVSQIAPG QTGNIADYNY KLPDDFTGCV IAWNSNKLDS KVSGNYNYLY
VLXT           DD

451      RLFRKSKLKP FERDISTEIY QAGNKPCNGV AGSNCYFPLQ SYGFRPTYGV
VLXT

501      GHQPYRVVVL SFELLHAPAT VCGPKKSTNL VKNKCVNFNF NGLTGTGVLT
VLXT

551      ESNKKFLPFQ QFGRDIADTT DAVRDPQTLE ILDITPCSFG GVSVITPGTN
VLXT                                                      DDD

601      TSNQVAVLYQ GVNCTEVPVA IHADQLTPTW RVYSTGSNVF QTRAGCLIGA
VLXT     DDDDDDD

651      EYVNNSYECD IPIGAGICAS YQTQTKSHRR ARSVASQSII AYTMSLGAEN
VLXT                               DDDDDD DDDDDDDDDD DDDDDDDDDD
```

```
701       SVAYSNNSIA IPTNFTISVT TEILPVSMTK TSVDCTMYIC GDSTECSNLL
VLXT      DDDDDD

751       LQYGSFCTQL KRALTGIAVE QDKNTQEVFA QVKQIYKTPP IKYFGGFNFS
VLXT

801       QILPDPSKPS KRSFIEDLLF NKVTLADAGF IKQYGDCLGD IAARDLICAQ
VLXT

851       KFNGLTVLPP LLTDEMIAQY TSALLAGTIT SGWTFGAGAA LQIPFAMQMA
VLXT                    DDD

901       YRFNGIGVTQ NVLYENQKLI ANQFNSAIGK IQDSLSSTAS ALGKLQDVVN
VLXT

951       HNAQALNTLV KQLSSKFGAI SSVLNDILSR LDKVEAEVQI DRLITGRLQS
VLXT                                  DD DDD     DD D

1001      LQTYVTQQLI RAAEIRASAN LAATKMSECV LGQSKRVDFC GKGYHLMSFP
VLXT                         D

1051      QSAPHGVVFL HVTYVPAQEK NFTTAPAICH DGKAHFPREG VFVSNGTHWF
VLXT

1101      VTQRNFYEPQ IITTDNTFVS GNCDVVIGIV NNTVYDPLQP ELDSFKEELD
VLXT

1151      KYFKNHTSPD VDLGDISGIN ASVVNIQKEI DRLNEVAKNL NESLINLQEL
VLXT                           DDDDDDDDDD DDDDDDDDDD D

1201      GKYEQYIKWP WYIWLGFIAG LIAIVMVTIM LCCMTSCCSC LKGCCSCGSC
VLXT

1251      CKFDEDDSEP VLKGVKLHYT
VLXT                D
```

Figure 11.5: *Intrinsically disordered predictions for the sequence of complete spike protein for BA.2.75.2 variant showing the ordered regions represented by " " and disordered regions represented by "D", analyzed using PONDR® VLXT.*

```
333       TNLCPFHEVF NATRFASVYA WNRKRISNCV ADYSVLYNFA PFFAFKCYGV
VLXT

383       SPTKLNDLCF TNVYADSFVI RGNEVSQIAP GQTGNIADYN YKLPDDFTGC
VLXT                                  DD

433       VIAWNSNKLD SKVSGNYNYL YRLFRKSKLK PFERDISTEI YQAGNKPCNG
VLXT

483       VAGFNCYFPL QSYGFRPTYG VGHQPYRVVV LSFELLHAPA TVCG
VLXT
```

Figure11.6: *Intrinsically disordered prediction for the sequence of RBD of spike protein for BA.2.75.2 variant showing the ordered regions represented by " " and disordered regions represented by "D", analyzed using PONDR® VLXT*

And for the Wild type, the ordered and disordered regions have been summarized in the **Table 11.6** and **Figure 7D.7 and 7D.8.**

Table 11.6*: Intrinsically disordered prediction for the complete sequence of wild type strain using PONDR® VLXT*

	No. of residues disordered	**Overall percent disordered**	**Predicted disordered segment**	**Average strength**	**Number of disordered regions**
Wild spike protein	98	7.70	[17]-[20]	0.5517	**11**
			[468]-[475]	0.5853	
			[601]-[608]	0.5639	
			[672]-[709]	0.8625	
			[869]-[871]	0.5518	
			[945]-[950]	0.5639	
			[982]-[986]	0.5240	
			[992]-[994]	0.5143	
			[1023]-[1023]	0.5047	
			[1174]-[1194]	0.6043	
			[1264]-[1264]	0.5035	

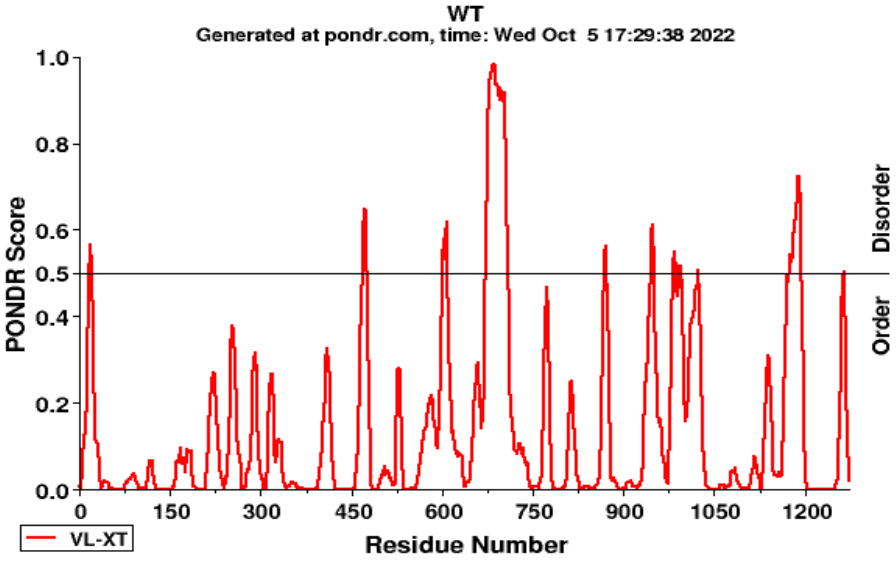

Figure 11.7: *PONDR score as a function of residue number analyzed for the complete sequence of wild type Wuhan strain using PONDR® VLXT*

```
1       MFVFLVLLPL VSSQCVNLTT RTQLPPAYTN SFTRGVYYPD KVFRSSVLHS
VLXT                    DDDD

51      TQDLFLPFFS NVTWFHAIHV SGTNGTKRFD NPVLPFNDGV YFASTEKSNI
VLXT

101     IRGWIFGTTL DSKTQSLLIV NNATNVVIKV CEFQFCNDPF LGVYYHKNNK
VLXT

151     SWMESEFRVY SSANNCTFEY VSQPFLMDLE GKQGNFKNLR EFVFKNIDGY
VLXT

201     FKIYSKHTPI NLVRDLPQGF SALEPLVDLP IGINITRFQT LLALHRSYLT
VLXT

251     PGDSSSGWTA GAAAYYVGYL QPRTFLLKYN ENGTITDAVD CALDPLSETK
VLXT

301     CTLKSFTVEK GIYQTSNFRV QPTESIVRFP NITNLCPFGE VFNATRFASV
VLXT

351     YAWNRKRISN CVADYSVLYN SASFSTFKCY GVSPTKLNDL CFTNVYADSF
VLXT

401     VIRGDEVRQI APGQTGKIAD YNYKLPDDFT GCVIAWNSNN LDSKVGGNYN
VLXT

451     YLYRLFRKSN LKPFERDIST EIYQAGSTPC NGVEGFNCYF PLQSYGFQPT
VLXT                    DDD DDDDD

501     NGVGYQPYRV VVLSFELLHA PATVCGPKKS TNLVKNKCVN FNFNGLTGTG
VLXT
```

```
551     VLTESNKKFL PFQQFGRDIA DTTDAVRDPQ TLEILDITPC SFGGVSVITP
VLXT

601     GTNTSNQVAV LYQDVNCTEV PVAIHADQLT PTWRVYSTGS NVFQTRAGCL
VLXT    DDDDDDDD

651     IGAEHVNNSY ECDIPIGAGI CASYQTQTNS PRRARSVASQ SIIAYTMSLG
VLXT                         DDDDDDDDD DDDDDDDDDD DDDDDDDDDD

701     AENSVAYSNN SIAIPTNFTI SVTTEILPVS MTKTSVDCTM YICGDSTECS
VLXT    DDDDDDDDD

751     NLLLQYGSFC TQLNRALTGI AVEQDKNTQE VFAQVKQIYK TPPIKDFGGF
VLXT

801     NFSQILPDPS KPSKRSFIED LLFNKVTLAD AGFIKQYGDC LGDIAARDLI
VLXT

851     CAQKFNGLTV LPPLLTDEMI AQYTSALLAG TITSGWTFGA GAALQIPFAM
VLXT                       DD D


901     QMAYRFNGIG VTQNVLYENQ KLIANQFNSA IGKIQDSLSS TASALGKLQD
VLXT                                                 DDDDDD

951     VVNQNAQALN TLVKQLSSNF GAISSVLNDI LSRLDKVEAE VQIDRLITGR
VLXT                                     DDDDD      DDD

1001    LQSLQTYVTQ QLIRAAEIRA SANLAATKMS ECVLGQSKRV DFCGKGYHLM
VLXT                             D

1051    SFPQSAPHGV VFLHVTYVPA QEKNFTTAPA ICHDGKAHFP REGVFVSNGT
VLXT

1101    HWFVTQRNFY EPQIITTDNT FVSGNCDVVI GIVNNTVYDP LQPELDSFKE
VLXT

1151    ELDKYFKNHT SPDVDLGDIS GINASVVNIQ KEIDRLNEVA KNLNESLIDL
VLXT                               DDDDDDD DDDDDDDDDD DDDD


1201    QELGKYEQYI KWPWYIWLGF IAGLIAIVMV TIMLCCMTSC CSCLKGCCSC
VLXT

1251    GSCCKFDEDD SEPVLKGVKL HYT
VLXT                  D
```

Figure 11.8: *Intrinsically disordered prediction for the complete sequence of spike protein for wild type Wuhan-Hu-1 strain showing the ordered regions represented by " " and disordered regions represented by "D", analyzed using PONDR® VLXT*

11.4.6. Prediction of protein stability changes upon mutation

I-Mutant3.0 is a tool that uses support vector machines (SVMs) to automatically forecast how single point mutations would affect protein stability. Both the protein structure and—more importantly—the

protein sequence are used as starting points for I-Mutant3.0 predictions and the values are depicted in the form of ΔΔG VALUE. I-Mutant analysis for the BA.2.75 and BA.2.75.2 variants were shown in **Table 11.7.**

Table 11.7. *I-mutant 3.0 analysis on the spike protein of the BA.2.75 and BA.2.75.2 variant*

RESIDUE NUMBER	OLD RESIDUE	NEW RESIDUE	ΔΔG VALUE (kcal/mol)
19	T	I	-0.20
142	G	D	-1.15
147	K	E	-0.68
152	W	R	-1.18
157	F	L	-1.09
210	I	V	-1.17
213	V	G	-2.86
257	G	S	-1.10
339	G	H	-1.41
346	***R***	***T***	***-0.99***
371	S	F	-0.15
373	S	P	-0.53
375	S	F	-0.33
376	T	A	-1.63
405	D	N	-0.92
408	R	S	-1.18
417	K	N	-0.42
440	N	K	-0.50
446	G	S	-1.49
460	N	K	-0.68
477	S	N	-0.45
478	T	K	-0.75
484	E	A	-0.79
486	***F***	***S***	***-1.76***
498	Q	R	-0.17
501	N	Y	0.15
505	Y	H	-1.49
614	D	G	-0.93
655	H	Y	0.08
679	N	K	-0.32
681	P	H	-1.27
764	N	K	-0.21
796	D	Y	-0.09
954	Q	H	-0.86
969	N	K	-0.63
1199	***D***	***N***	***-0.68***

ΔΔG< 0; Decrease stability
ΔΔG> 0; Increase stability
ΔΔG< -0.5; Large decrease of stability
ΔΔG> 0.5; Large increase of stability
-0.5 <=ΔΔG<= 0.5

And it was seen that N501Y and H655Y mutations increases the stability of the protein with ΔΔG> 0 kcal/mol whereas the other mutated residues are seen to have ΔΔG< 0. And the residues ***(texted in italics and bold)*** are exclusively present in BA.2.75.2 variant.

11.4.7. Determination of the interface interactions of the S protein (BA.2.75)-ACE2 and S protein (BA.2.75.2)-ACE2 complex.

An interface area is usually defined as a region where two sets of proteins come in contact with each other. Surface residues with large surface regions accessible to the solvent available usually characterize them. The interface statistics for both the complexes (BA.2.75/BA.2.75.2)-ACE2 complexes were obtained upon the submission of their 3-D structure to the PDBsum server. The interface statistics for the two complexes have been summarised in **Table 11.8**.

Table 11.8. *Interface statistics for the S protein (BA.2.75)-ACE2 and S protein (BA.2.75.2)-ACE2 complexes*

Complex System	Chain	No. of Interface Residues	Interface area (Å^2)	No. of Salt Bridges	No. of Disulphide Bonds	No. of Hydrogen bonds	No. of Non-Bonded Contacts
S protein (BA.2.75)-ACE2	ACE2	19	820	-	-	9	154
	SPIKE (BA.2.75)	18	913				
S protein (BA.2.75.2)-ACE2	ACE2	18	787			9	145
	SPIKE (BA.2.75.2)	17	864				

In the S protein (BA.2.75)-ACE2 complex, the interface area for the S protein chain and the ACE2 chain involved in the interaction was observed to be 820 Å^2 and 913 Å^2 respectively and that for the S protein (BA.2.75.2)-ACE2 was found to be 787 Å^2 and 864 Å^2 respectively. Both the complexes are stabilized by molecular interactions like hydrogen bonding, and non-bonded contacts.

From **Table 7D.8**, we can see the presence of nine hydrogen bonds and one hundred and fifty-four non-bonded contacts at the interface of S protein (BA.2.75) and ACE2 in the S protein (BA.2.75)-ACE2 complex. However,

at the interface of S protein (BA.2.75.2) and ACE2 in the S protein (BA.2.75.2)-ACE2 complex, we observed one hundred and forty-five non-bonded contacts and nine hydrogen bonds. Overall, we see the number of intermolecular interactions and the interface area shared by S protein and ACE2 in forming complex is larger in S protein (BA.2.75)-ACE2 complex than in the S protein (BA.2.75.2)-ACE2 complex. Therefore, the stability of S protein-CAT complex was found to be higher than the S protein-L-SIGN complex. From our earlier study, in the case of S protein (wild)-ACE2 complex, we noticed the complex to contain one salt bridge, eight hydrogen bonds and one hundred and fifteen non-bonded contacts [58].

The list of atom-atom interactions (Hydrogen bonds and non-bonded contacts) across protein-protein interface in ACE2 (chain A)-S Protein (Chain B) (BA.2.75 variant) complex from PDBsum server is shown in **Table 11.9 and 11.10**. And the list of atom-atom interactions (Hydrogen bonds and non-bonded contacts) across protein-ligand interface in ACE2 (chain A)-S Protein (Chain B) (BA.2.75.2 variant) complex from PDBsum server is shown in supplementary **Table 11.11 and 11.12.**

Table 11.9. *List of atom-atom interactions (Hydrogen bonds) across protein-ligand interface in ACE2 (chain A)-Spike Protein (Chain B) (BA.2.75 variant) complex from PDBsum server*

ACE2 Receptor							Spike Protein					
Sl.no.	Atom no.	Atom name	Res name	Res no.	Chain	Hydrogen bonds	Atom no.	Atom name	Res name	Res no.	Chain	Distance
1	6	OG	SER	19	A	<-->	6025	O	ALA	475	B	2.81
2	48	NE2	GLN	24	A	<-->	6106	OD1	ASN	487	B	2.87
3	165	OD2	ASP	38	A	<-->	5794	OH	TYR	449	B	2.83
4	196	OH	TYR	41	A	<-->	6217	OG1	THR	500	B	2.73
5	196	OH	TYR	41	A	<-->	6217	OG1	THR	500	B	2.73
6	204	OE1	GLN	42	A	<-->	5794	OH	TYR	449	B	3.09
7	534	OH	TYR	83	A	<-->	6107	ND2	ASN	487	B	2.82
8	2720	O	LYS	353	A	<-->	6231	N	GLY	502	B	2.79
9	2725	NZ	LYS	353	A	<-->	6182	O	GLY	496	B	3.22

Table 11.10. *List of atom-atom interactions (Non-bonded contacts) across protein-ligand interface in ACE2 (chain A)-Spike Protein (Chain B) (BA.2.75variant) complex from PDBsum server*

ACE2 Receptor							Spike Protein					
Sl.no	Atom no.	Atom name	Res name	Res no.	Chain	Non-bonded contacts	Atom no.	Atom name	Res name	Res no.	Chain	Distance
1	5	CB	SER	19	A	<-->	6025	O	ALA	475	B	3.62
2	6	OG	SER	19	A	<-->	6024	C	ALA	475	B	3.89
3	6	OG	SER	19	A	<-->	6025	O	ALA	475	B	2.81
4	6	OG	SER	19	A	<-->	6028	CA	GLY	476	B	3.81
5	44	CB	GLN	24	A	<-->	6107	ND2	ASN	487	B	3.82
6	45	CG	GLN	24	A	<-->	6025	O	ALA	475	B	3.89

7	45	CG	GLN	24	A	<-->	6105	CG	ASN	487	B	3.48
8	45	CG	GLN	24	A	<-->	6106	OD1	ASN	487	B	3.25
9	45	CG	GLN	24	A	<-->	6107	ND2	ASN	487	B	3.24
10	46	CD	GLN	24	A	<-->	6106	OD1	ASN	487	B	3.38
11	48	NE2	GLN	24	A	<-->	6105	CG	ASN	487	B	3.83
12	48	NE2	GLN	24	A	<-->	6106	OD1	ASN	487	B	2.87
13	66	O	THR	27	A	<-->	5864	CZ	PHE	456	B	3.77
14	69	CG2	THR	27	A	<-->	5862	CE1	PHE	456	B	3.53
15	69	CG2	THR	27	A	<-->	6123	CE2	TYR	489	B	3.62
16	70	N	PHE	28	A	<-->	6125	OH	TYR	489	B	3.83
17	71	CA	PHE	28	A	<-->	6125	OH	TYR	489	B	3.36
18	74	CB	PHE	28	A	<-->	6125	OH	TYR	489	B	3.4
19	76	CD1	PHE	28	A	<-->	6125	OH	TYR	489	B	3.84
20	93	CB	ASP	30	A	<-->	5862	CE1	PHE	456	B	3.87
21	105	NZ	LYS	31	A	<-->	6129	O	PHE	490	B	3.82
22	127	C	HIS	34	A	<-->	6160	NE2	GLN	493	B	3.53
23	128	O	HIS	34	A	<-->	6160	NE2	GLN	493	B	3.52
24	129	CB	HIS	34	A	<-->	6160	NE2	GLN	493	B	3.53
25	130	CG	HIS	34	A	<-->	5834	OH	TYR	453	B	3.72
26	131	ND1	HIS	34	A	<-->	5852	CD1	LEU	455	B	3.71
27	132	CD2	HIS	34	A	<-->	5834	OH	TYR	453	B	2.93
28	132	CD2	HIS	34	A	<-->	5852	CD1	LEU	455	B	3.8
29	133	CE1	HIS	34	A	<-->	5852	CD1	LEU	455	B	3.34
30	134	NE2	HIS	34	A	<-->	5834	OH	TYR	453	B	3.79
31	134	NE2	HIS	34	A	<-->	5852	CD1	LEU	455	B	3.37
32	135	N	GLU	35	A	<-->	6160	NE2	GLN	493	B	3.77
33	141	CD	GLU	35	A	<-->	6160	NE2	GLN	493	B	3.77
34	142	OE1	GLU	35	A	<-->	6160	NE2	GLN	493	B	3.39
35	143	OE2	GLU	35	A	<-->	6159	OE1	GLN	493	B	3.68
36	143	OE2	GLU	35	A	<-->	6160	NE2	GLN	493	B	3.87
37	163	CG	ASP	38	A	<-->	5794	OH	TYR	449	B	3.55
38	164	OD1	ASP	38	A	<-->	5794	OH	TYR	449	B	3.51
39	164	OD1	ASP	38	A	<-->	6230	OH	TYR	501	B	3.42
40	165	OD2	ASP	38	A	<-->	5792	CE2	TYR	449	B	3.57
41	165	OD2	ASP	38	A	<-->	5793	CZ	TYR	449	B	3.65
42	165	OD2	ASP	38	A	<-->	5794	OH	TYR	449	B	2.83
43	190	CG	TYR	41	A	<-->	6229	CE1	TYR	501	B	3.79
44	190	CG	TYR	41	A	<-->	6230	OH	TYR	501	B	3.88
45	191	CD1	TYR	41	A	<-->	6229	CE1	TYR	501	B	3.85
46	192	CD2	TYR	41	A	<-->	6200	CD	ARG	498	B	3.74
47	192	CD2	TYR	41	A	<-->	6204	NH1	ARG	498	B	3.52
48	192	CD2	TYR	41	A	<-->	6229	CE1	TYR	501	B	3.6
49	192	CD2	TYR	41	A	<-->	6228	CZ	TYR	501	B	3.53
50	192	CD2	TYR	41	A	<-->	6230	OH	TYR	501	B	3.18

51	193	CE1	TYR	41	A	<-->	6229	CE1	TYR	501	B	3.76
52	194	CE2	TYR	41	A	<-->	6200	CD	ARG	498	B	3.48
53	194	CE2	TYR	41	A	<-->	6229	CE1	TYR	501	B	3.5
54	194	CE2	TYR	41	A	<-->	6228	CZ	TYR	501	B	3.4
55	194	CE2	TYR	41	A	<-->	6230	OH	TYR	501	B	3.5
56	195	CZ	TYR	41	A	<-->	6217	OG1	THR	500	B	3.85
57	195	CZ	TYR	41	A	<-->	6225	CD1	TYR	501	B	3.83
58	195	CZ	TYR	41	A	<-->	6229	CE1	TYR	501	B	3.58
59	196	OH	TYR	41	A	<-->	6214	C	THR	500	B	3.43
60	196	OH	TYR	41	A	<-->	6215	O	THR	500	B	3.51
61	196	OH	TYR	41	A	<-->	6216	CB	THR	500	B	3.46
62	196	OH	TYR	41	A	<-->	6217	OG1	THR	500	B	2.73
63	196	OH	TYR	41	A	<-->	6219	N	TYR	501	B	3.62
64	197	N	GLN	42	A	<-->	6204	NH1	ARG	498	B	3.81
65	198	CA	GLN	42	A	<-->	6204	NH1	ARG	498	B	3.33
66	201	CB	GLN	42	A	<-->	6204	NH1	ARG	498	B	3.9
67	201	CB	GLN	42	A	<-->	6203	NH2	ARG	498	B	3.62
68	202	CG	GLN	42	A	<-->	6202	CZ	ARG	498	B	3.4
69	202	CG	GLN	42	A	<-->	6204	NH1	ARG	498	B	3.58
70	202	CG	GLN	42	A	<-->	6203	NH2	ARG	498	B	2.58
71	203	CD	GLN	42	A	<-->	6201	NE	ARG	498	B	3.24
72	203	CD	GLN	42	A	<-->	6202	CZ	ARG	498	B	2.09
73	203	CD	GLN	42	A	<-->	6204	NH1	ARG	498	B	2.55
74	203	CD	GLN	42	A	<-->	6203	NH2	ARG	498	B	1.14
75	204	OE1	GLN	42	A	<-->	5768	O	SER	446	B	3.34
76	204	OE1	GLN	42	A	<-->	5794	OH	TYR	449	B	3.09
77	204	OE1	GLN	42	A	<-->	6200	CD	ARG	498	B	3.88
78	204	OE1	GLN	42	A	<-->	6201	NE	ARG	498	B	2.47
79	204	OE1	GLN	42	A	<-->	6202	CZ	ARG	498	B	1.73
80	204	OE1	GLN	42	A	<-->	6204	NH1	ARG	498	B	2.75
81	204	OE1	GLN	42	A	<-->	6203	NH2	ARG	498	B	0.74
82	205	NE2	GLN	42	A	<-->	6201	NE	ARG	498	B	3.5
83	205	NE2	GLN	42	A	<-->	6202	CZ	ARG	498	B	2.24
84	205	NE2	GLN	42	A	<-->	6204	NH1	ARG	498	B	2.29
85	205	NE2	GLN	42	A	<-->	6203	NH2	ARG	498	B	1.66
86	225	CD2	LEU	45	A	<-->	6200	CD	ARG	498	B	3.87
87	225	CD2	LEU	45	A	<-->	6204	NH1	ARG	498	B	3.11
88	519	CB	MET	82	A	<-->	6097	CE1	PHE	486	B	3.63
89	521	SD	MET	82	A	<-->	6095	CD1	PHE	486	B	3.66
90	521	SD	MET	82	A	<-->	6097	CE1	PHE	486	B	3.75
91	531	CE1	TYR	83	A	<-->	6099	CZ	PHE	486	B	3.79
92	531	CE1	TYR	83	A	<-->	6107	ND2	ASN	487	B	3.86
93	532	CE2	TYR	83	A	<-->	6097	CE1	PHE	486	B	3.79
94	533	CZ	TYR	83	A	<-->	6097	CE1	PHE	486	B	3.48

95	533	CZ	TYR	83	A	<-->	6099	CZ	PHE	486	B	3.69
96	533	CZ	TYR	83	A	<-->	6107	ND2	ASN	487	B	3.79
97	534	OH	TYR	83	A	<-->	6097	CE1	PHE	486	B	3.33
98	534	OH	TYR	83	A	<-->	6099	CZ	PHE	486	B	3.69
99	534	OH	TYR	83	A	<-->	6105	CG	ASN	487	B	3.65
100	534	OH	TYR	83	A	<-->	6107	ND2	ASN	487	B	2.82
101	534	OH	TYR	83	A	<-->	6125	OH	TYR	489	B	3.54
102	2553	OD1	ASN	330	A	<-->	6218	CG2	THR	500	B	3.53
103	2717	N	LYS	353	A	<-->	6254	NE2	HIS	505	B	3.85
104	2718	CA	LYS	353	A	<-->	6251	CG	HIS	505	B	3.47
105	2718	CA	LYS	353	A	<-->	6252	ND1	HIS	505	B	3.88
106	2718	CA	LYS	353	A	<-->	6253	CD2	HIS	505	B	2.89
107	2718	CA	LYS	353	A	<-->	6255	CE1	HIS	505	B	3.63
108	2718	CA	LYS	353	A	<-->	6254	NE2	HIS	505	B	3.03
109	2719	C	LYS	353	A	<-->	6251	CG	HIS	505	B	3.38
110	2719	C	LYS	353	A	<-->	6253	CD2	HIS	505	B	2.46
111	2719	C	LYS	353	A	<-->	6254	NE2	HIS	505	B	3.02
112	2720	O	LYS	353	A	<-->	6220	CA	TYR	501	B	3.58
113	2720	O	LYS	353	A	<-->	6221	C	TYR	501	B	3.66
114	2720	O	LYS	353	A	<-->	6223	CB	TYR	501	B	3.67
115	2720	O	LYS	353	A	<-->	6225	CD1	TYR	501	B	3.54
116	2720	O	LYS	353	A	<-->	6231	N	GLY	502	B	2.79
117	2720	O	LYS	353	A	<-->	6232	CA	GLY	502	B	3.68
118	2720	O	LYS	353	A	<-->	6250	CB	HIS	505	B	3.58
119	2720	O	LYS	353	A	<-->	6251	CG	HIS	505	B	3.27
120	2720	O	LYS	353	A	<-->	6253	CD2	HIS	505	B	2.63
121	2720	O	LYS	353	A	<-->	6254	NE2	HIS	505	B	3.63
122	2721	CB	LYS	353	A	<-->	6224	CG	TYR	501	B	3.89
123	2721	CB	LYS	353	A	<-->	6225	CD1	TYR	501	B	2.59
124	2721	CB	LYS	353	A	<-->	6229	CE1	TYR	501	B	2.87
125	2721	CB	LYS	353	A	<-->	6251	CG	HIS	505	B	3.85
126	2721	CB	LYS	353	A	<-->	6253	CD2	HIS	505	B	3.75
127	2722	CG	LYS	353	A	<-->	6225	CD1	TYR	501	B	3.14
128	2722	CG	LYS	353	A	<-->	6229	CE1	TYR	501	B	2.8
129	2723	CD	LYS	353	A	<-->	6225	CD1	TYR	501	B	2.85
130	2723	CD	LYS	353	A	<-->	6229	CE1	TYR	501	B	1.86
131	2723	CD	LYS	353	A	<-->	6228	CZ	TYR	501	B	2.75
132	2723	CD	LYS	353	A	<-->	6230	OH	TYR	501	B	2.95
133	2724	CE	LYS	353	A	<-->	6229	CE1	TYR	501	B	2.87
134	2724	CE	LYS	353	A	<-->	6228	CZ	TYR	501	B	3.19
135	2724	CE	LYS	353	A	<-->	6230	OH	TYR	501	B	2.93
136	2725	NZ	LYS	353	A	<-->	6182	O	GLY	496	B	3.22
137	2725	NZ	LYS	353	A	<-->	6229	CE1	TYR	501	B	3.21
138	2725	NZ	LYS	353	A	<-->	6228	CZ	TYR	501	B	3.36

139	2725	NZ	LYS	353	A	<-->	6230	OH	TYR	501	B	3.39
140	2726	N	GLY	354	A	<-->	6253	CD2	HIS	505	B	2.95
141	2726	N	GLY	354	A	<-->	6254	NE2	HIS	505	B	3.18
142	2727	CA	GLY	354	A	<-->	6253	CD2	HIS	505	B	3.59
143	2728	C	GLY	354	A	<-->	6231	N	GLY	502	B	3.69
144	2728	C	GLY	354	A	<-->	6232	CA	GLY	502	B	3.87
145	2729	O	GLY	354	A	<-->	6231	N	GLY	502	B	3.61
146	2729	O	GLY	354	A	<-->	6232	CA	GLY	502	B	3.45
147	2734	CB	ASP	355	A	<-->	6215	O	THR	500	B	3.8
148	2735	CG	ASP	355	A	<-->	6215	O	THR	500	B	3.54
149	2737	OD2	ASP	355	A	<-->	6215	O	THR	500	B	3.36
150	2737	OD2	ASP	355	A	<-->	6216	CB	THR	500	B	3.75
151	2737	OD2	ASP	355	A	<-->	6217	OG1	THR	500	B	3.86
152	2759	NH2	ARG	357	A	<-->	6216	CB	THR	500	B	3.43
153	2759	NH2	ARG	357	A	<-->	6217	OG1	THR	500	B	3.66
154	2759	NH2	ARG	357	A	<-->	6218	CG2	THR	500	B	3.57

Table 11.11. *List of atom-atom interactions (Hydrogen bonds) across protein-ligand interface in ACE2 (chain A)-Spike Protein (Chain B) (BA.2.75.2 variant) complex from PDBsum server*

ACE2 Receptor						Hydrogen bonds	Spike protein (BA.2.75.2)					
Sl.no	Atom no.	Atom name	Res name	Res no.	Chain		Atom no.	Atom name	Res name	Res no.	Chain	Distance
1	6	OG	SER	19	A	<-->	6021	O	ALA	475	B	2.81
2	48	NE2	GLN	24	A	<-->	6097	OD1	ASN	487	B	2.87
3	165	OD2	ASP	38	A	<-->	5790	OH	TYR	449	B	2.83
4	196	OH	TYR	41	A	<-->	6208	OG1	THR	500	B	2.73
5	196	OH	TYR	41	A	<-->	6208	OG1	THR	500	B	2.73
6	204	OE1	GLN	42	A	<-->	5790	OH	TYR	449	B	3.09
7	534	OH	TYR	83	A	<-->	6098	ND2	ASN	487	B	2.82
8	2720	O	LYS	353	A	<-->	6222	N	GLY	502	B	2.79
9	2725	NZ	LYS	353	A	<-->	6173	O	GLY	496	B	3.22

Table 11.12. *List of atom-atom interactions (Non-bonded contacts) across protein-ligand interface in ACE2 (chain A)-Spike Protein (Chain B) (BA.2.75.2 variant) complex from PDBsum server*

ACE2 Receptor						Non-bonded bonds	Spike protein (BA.2.75.2)					
Sl.no	Atom no.	Atom name	Res name	Res no.	Chain		Atom no.	Atom name	Res name	Res no.	Chain	Distance
1	5	CB	SER	19	A	<-->	6021	O	ALA	475	B	3.62
2	6	OG	SER	19	A	<-->	6020	C	ALA	475	B	3.89
3	6	OG	SER	19	A	<-->	6021	O	ALA	475	B	2.81
4	6	OG	SER	19	A	<-->	6024	CA	GLY	476	B	3.81
5	44	CB	GLN	24	A	<-->	6098	ND2	ASN	487	B	3.82

6	45	CG	GLN	24	A	<-->	6021	O	ALA	475	B	3.89
7	45	CG	GLN	24	A	<-->	6096	CG	ASN	487	B	3.48
8	45	CG	GLN	24	A	<-->	6097	OD1	ASN	487	B	3.25
9	45	CG	GLN	24	A	<-->	6098	ND2	ASN	487	B	3.24
10	46	CD	GLN	24	A	<-->	6097	OD1	ASN	487	B	3.38
11	48	NE2	GLN	24	A	<-->	6096	CG	ASN	487	B	3.83
12	48	NE2	GLN	24	A	<-->	6097	OD1	ASN	487	B	2.87
13	66	O	THR	27	A	<-->	5860	CZ	PHE	456	B	3.77
14	69	CG2	THR	27	A	<-->	5858	CE1	PHE	456	B	3.53
15	69	CG2	THR	27	A	<-->	6114	CE2	TYR	489	B	3.62
16	70	N	PHE	28	A	<-->	6116	OH	TYR	489	B	3.83
17	71	CA	PHE	28	A	<-->	6116	OH	TYR	489	B	3.36
18	74	CB	PHE	28	A	<-->	6116	OH	TYR	489	B	3.4
19	76	CD1	PHE	28	A	<-->	6116	OH	TYR	489	B	3.84
20	93	CB	ASP	30	A	<-->	5858	CE1	PHE	456	B	3.87
21	105	NZ	LYS	31	A	<-->	6120	O	PHE	490	B	3.82
22	127	C	HIS	34	A	<-->	6151	NE2	GLN	493	B	3.53
23	128	O	HIS	34	A	<-->	6151	NE2	GLN	493	B	3.52
24	129	CB	HIS	34	A	<-->	6151	NE2	GLN	493	B	3.53
25	130	CG	HIS	34	A	<-->	5830	OH	TYR	453	B	3.72
26	131	ND1	HIS	34	A	<-->	5848	CD1	LEU	455	B	3.71
27	132	CD2	HIS	34	A	<-->	5830	OH	TYR	453	B	2.93
28	132	CD2	HIS	34	A	<-->	5848	CD1	LEU	455	B	3.8
29	133	CE1	HIS	34	A	<-->	5848	CD1	LEU	455	B	3.34
30	134	NE2	HIS	34	A	<-->	5830	OH	TYR	453	B	3.79
31	134	NE2	HIS	34	A	<-->	5848	CD1	LEU	455	B	3.37
32	135	N	GLU	35	A	<-->	6151	NE2	GLN	493	B	3.77
33	141	CD	GLU	35	A	<-->	6151	NE2	GLN	493	B	3.77
34	142	OE1	GLU	35	A	<-->	6151	NE2	GLN	493	B	3.39
35	143	OE2	GLU	35	A	<-->	6150	OE1	GLN	493	B	3.68
36	143	OE2	GLU	35	A	<-->	6151	NE2	GLN	493	B	3.87
37	163	CG	ASP	38	A	<-->	5790	OH	TYR	449	B	3.55
38	164	OD1	ASP	38	A	<-->	5790	OH	TYR	449	B	3.51
39	164	OD1	ASP	38	A	<-->	6221	OH	TYR	501	B	3.42
40	165	OD2	ASP	38	A	<-->	5788	CE2	TYR	449	B	3.57
41	165	OD2	ASP	38	A	<-->	5789	CZ	TYR	449	B	3.65
42	165	OD2	ASP	38	A	<-->	5790	OH	TYR	449	B	2.83
43	190	CG	TYR	41	A	<-->	6220	CE1	TYR	501	B	3.79
44	190	CG	TYR	41	A	<-->	6221	OH	TYR	501	B	3.88
45	191	CD1	TYR	41	A	<-->	6220	CE1	TYR	501	B	3.85
46	192	CD2	TYR	41	A	<-->	6191	CD	ARG	498	B	3.74
47	192	CD2	TYR	41	A	<-->	6195	NH1	ARG	498	B	3.52
48	192	CD2	TYR	41	A	<-->	6220	CE1	TYR	501	B	3.6
49	192	CD2	TYR	41	A	<-->	6219	CZ	TYR	501	B	3.53

50	192	CD2	TYR	41	A	<-->	6221	OH	TYR	501	B	3.18
51	193	CE1	TYR	41	A	<-->	6220	CE1	TYR	501	B	3.76
52	194	CE2	TYR	41	A	<-->	6191	CD	ARG	498	B	3.48
53	194	CE2	TYR	41	A	<-->	6220	CE1	TYR	501	B	3.5
54	194	CE2	TYR	41	A	<-->	6219	CZ	TYR	501	B	3.4
55	194	CE2	TYR	41	A	<-->	6221	OH	TYR	501	B	3.5
56	195	CZ	TYR	41	A	<-->	6208	OG1	THR	500	B	3.85
57	195	CZ	TYR	41	A	<-->	6216	CD1	TYR	501	B	3.83
58	195	CZ	TYR	41	A	<-->	6220	CE1	TYR	501	B	3.58
59	196	OH	TYR	41	A	<-->	6205	C	THR	500	B	3.43
60	196	OH	TYR	41	A	<-->	6206	O	THR	500	B	3.51
61	196	OH	TYR	41	A	<-->	6207	CB	THR	500	B	3.46
62	196	OH	TYR	41	A	<-->	6208	OG1	THR	500	B	2.73
63	196	OH	TYR	41	A	<-->	6210	N	TYR	501	B	3.62
64	197	N	GLN	42	A	<-->	6195	NH1	ARG	498	B	3.81
65	198	CA	GLN	42	A	<-->	6195	NH1	ARG	498	B	3.33
66	201	CB	GLN	42	A	<-->	6195	NH1	ARG	498	B	3.9
67	201	CB	GLN	42	A	<-->	6194	NH2	ARG	498	B	3.62
68	202	CG	GLN	42	A	<-->	6193	CZ	ARG	498	B	3.4
69	202	CG	GLN	42	A	<-->	6195	NH1	ARG	498	B	3.58
70	202	CG	GLN	42	A	<-->	6194	NH2	ARG	498	B	2.58
71	203	CD	GLN	42	A	<-->	6192	NE	ARG	498	B	3.24
72	203	CD	GLN	42	A	<-->	6193	CZ	ARG	498	B	2.09
73	203	CD	GLN	42	A	<-->	6195	NH1	ARG	498	B	2.55
74	203	CD	GLN	42	A	<-->	6194	NH2	ARG	498	B	1.14
75	204	OE1	GLN	42	A	<-->	5764	O	SER	446	B	3.34
76	204	OE1	GLN	42	A	<-->	5790	OH	TYR	449	B	3.09
77	204	OE1	GLN	42	A	<-->	6191	CD	ARG	498	B	3.88
78	204	OE1	GLN	42	A	<-->	6192	NE	ARG	498	B	2.47
79	204	OE1	GLN	42	A	<-->	6193	CZ	ARG	498	B	1.73
80	204	OE1	GLN	42	A	<-->	6195	NH1	ARG	498	B	2.75
81	204	OE1	GLN	42	A	<-->	6194	NH2	ARG	498	B	0.74
82	205	NE2	GLN	42	A	<-->	6192	NE	ARG	498	B	3.5
83	205	NE2	GLN	42	A	<-->	6193	CZ	ARG	498	B	2.24
84	205	NE2	GLN	42	A	<-->	6195	NH1	ARG	498	B	2.29
85	205	NE2	GLN	42	A	<-->	6194	NH2	ARG	498	B	1.66
86	225	CD2	LEU	45	A	<-->	6191	CD	ARG	498	B	3.87
87	225	CD2	LEU	45	A	<-->	6195	NH1	ARG	498	B	3.11
88	531	CE1	TYR	83	A	<-->	6098	ND2	ASN	487	B	3.86
89	533	CZ	TYR	83	A	<-->	6098	ND2	ASN	487	B	3.79
90	534	OH	TYR	83	A	<-->	6096	CG	ASN	487	B	3.65
91	534	OH	TYR	83	A	<-->	6098	ND2	ASN	487	B	2.82
92	534	OH	TYR	83	A	<-->	6116	OH	TYR	489	B	3.54
93	2553	OD1	ASN	330	A	<-->	6209	CG2	THR	500	B	3.53

94	2717	N	LYS	353	A	<-->	6245	NE2	HIS	505	B	3.85
95	2718	CA	LYS	353	A	<-->	6242	CG	HIS	505	B	3.47
96	2718	CA	LYS	353	A	<-->	6243	ND1	HIS	505	B	3.88
97	2718	CA	LYS	353	A	<-->	6244	CD2	HIS	505	B	2.89
98	2718	CA	LYS	353	A	<-->	6246	CE1	HIS	505	B	3.63
99	2718	CA	LYS	353	A	<-->	6245	NE2	HIS	505	B	3.03
100	2719	C	LYS	353	A	<-->	6242	CG	HIS	505	B	3.38
101	2719	C	LYS	353	A	<-->	6244	CD2	HIS	505	B	2.46
102	2719	C	LYS	353	A	<-->	6245	NE2	HIS	505	B	3.02
103	2720	O	LYS	353	A	<-->	6211	CA	TYR	501	B	3.58
104	2720	O	LYS	353	A	<-->	6212	C	TYR	501	B	3.66
105	2720	O	LYS	353	A	<-->	6214	CB	TYR	501	B	3.67
106	2720	O	LYS	353	A	<-->	6216	CD1	TYR	501	B	3.54
107	2720	O	LYS	353	A	<-->	6222	N	GLY	502	B	2.79
108	2720	O	LYS	353	A	<-->	6223	CA	GLY	502	B	3.68
109	2720	O	LYS	353	A	<-->	6241	CB	HIS	505	B	3.58
110	2720	O	LYS	353	A	<-->	6242	CG	HIS	505	B	3.27
111	2720	O	LYS	353	A	<-->	6244	CD2	HIS	505	B	2.63
112	2720	O	LYS	353	A	<-->	6245	NE2	HIS	505	B	3.63
113	2721	CB	LYS	353	A	<-->	6215	CG	TYR	501	B	3.89
114	2721	CB	LYS	353	A	<-->	6216	CD1	TYR	501	B	2.59
115	2721	CB	LYS	353	A	<-->	6220	CE1	TYR	501	B	2.87
116	2721	CB	LYS	353	A	<-->	6242	CG	HIS	505	B	3.85
117	2721	CB	LYS	353	A	<-->	6244	CD2	HIS	505	B	3.75
118	2722	CG	LYS	353	A	<-->	6216	CD1	TYR	501	B	3.14
119	2722	CG	LYS	353	A	<-->	6220	CE1	TYR	501	B	2.8
120	2723	CD	LYS	353	A	<-->	6216	CD1	TYR	501	B	2.85
121	2723	CD	LYS	353	A	<-->	6220	CE1	TYR	501	B	1.86
122	2723	CD	LYS	353	A	<-->	6219	CZ	TYR	501	B	2.75
123	2723	CD	LYS	353	A	<-->	6221	OH	TYR	501	B	2.95
124	2724	CE	LYS	353	A	<-->	6220	CE1	TYR	501	B	2.87
125	2724	CE	LYS	353	A	<-->	6219	CZ	TYR	501	B	3.19
126	2724	CE	LYS	353	A	<-->	6221	OH	TYR	501	B	2.93
127	2725	NZ	LYS	353	A	<-->	6173	O	GLY	496	B	3.22
128	2725	NZ	LYS	353	A	<-->	6220	CE1	TYR	501	B	3.21
129	2725	NZ	LYS	353	A	<-->	6219	CZ	TYR	501	B	3.36
130	2725	NZ	LYS	353	A	<-->	6221	OH	TYR	501	B	3.39
131	2726	N	GLY	354	A	<-->	6244	CD2	HIS	505	B	2.95
132	2726	N	GLY	354	A	<-->	6245	NE2	HIS	505	B	3.18
133	2727	CA	GLY	354	A	<-->	6244	CD2	HIS	505	B	3.59
134	2728	C	GLY	354	A	<-->	6222	N	GLY	502	B	3.69
135	2728	C	GLY	354	A	<-->	6223	CA	GLY	502	B	3.87
136	2729	O	GLY	354	A	<-->	6222	N	GLY	502	B	3.61
137	2729	O	GLY	354	A	<-->	6223	CA	GLY	502	B	3.45

138	2734	CB	ASP	355	A	<-->	6206	O	THR	500	B	3.8
139	2735	CG	ASP	355	A	<-->	6206	O	THR	500	B	3.54
140	2737	OD2	ASP	355	A	<-->	6206	O	THR	500	B	3.36
141	2737	OD2	ASP	355	A	<-->	6207	CB	THR	500	B	3.75
142	2737	OD2	ASP	355	A	<-->	6208	OG1	THR	500	B	3.86
143	2759	NH2	ARG	357	A	<-->	6207	CB	THR	500	B	3.43
144	2759	NH2	ARG	357	A	<-->	6208	OG1	THR	500	B	3.66
145	2759	NH2	ARG	357	A	<-->	6209	CG2	THR	500	B	3.57

11.4.8. Effect of protein functioning upon mutations

SIFT analysis revealed that in the BA.2.75 variant, the mutations Y505H and N764K impairs protein function and an increased risk of disease as shown in **Table 11.13 and 11.14**. Other mutations, such as G339H, S371F, S373P, T376A D405N, R408S, K417N, N440K, G446S, N460K, S477N, T478K, E484A, and Q498R are tolerated and doesn't affect the protein function as shown in **Table 11.13** while in BA.2.75.2, the three mutations (Y505H and N764K, D1199N) were observed to impair the protein function as shown in **Table 11.14.**

Table 11.13. *SIFT analysis for BA.2.75 variant*

Sl.no	**Residue no.**	**Tolerance/ intolerance score**	**AFFECT PROTEIN FUNCTION (intolerance)**	**DOESN'T AFFECT PROTEIN FUNCTION (tolerance)**	**Seq Rep**
1.	T19I	0.10	no	yes	0.56
2.	G142D	0.18	no	yes	0.67
3.	K147E	0.86	no	yes	0.56
4.	W152R	0.17	no	yes	0.67
5.	F157L	0.75	no	yes	0.33
6.	I210V	1.00	no	yes	0.67
7.	V213G	0.25	no	yes	0.67
8.	G257S	0.85	no	yes	0.78
9.	G339H	0.16	no	yes	1.00
10.	S371F	0.26	no	yes	1.00
11.	S373P	0.38	no	yes	1.00
12.	S375F	**0.07**	no	yes	1.00
13.	T376A	0.33	no	yes	1.00
14.	D405N	0.27	no	yes	1.00
15.	R408S	0.87	no	yes	1.00
16.	K417N	0.56	no	yes	1.00
17.	N440K	0.70	no	yes	0.89
18.	G446S	0.79	no	yes	0.44
19	N460K	1.00	no	yes	0.78
20.	S477N	0.84	no	yes	0.44
21	T478K	0.75	no	yes	0.44
22.	E484A	0.51	no	yes	0.56

23.	Q498R	0.39	no	yes	0.78
24.	N501Y	0.09	no	yes	0.89
25.	***Y505H***	***0.03***	***yes***	***no***	***0.89***
26.	D614G	0.62	no	yes	1.00
27.	H655Y	0.50	no	yes	0.78
28.	N679K	0.53	no	yes	0.67
29.	P681H	0.17	no	yes	0.56
30.	***N764K***	***0.00***	***yes***	***no***	***1.00***
31.	D796Y	1.00	no	yes	1.00
32.	Q954H	0.08	no	yes	1.00
33.	N969K	0.09	no	yes	1.00

- ***Residues in italics and bold impairs protein function and caused an increased risk of disease.***

Table 11.14. *SIFT analysis for BA.2.75.2 variant*

Sl.no	**Residue no.**	**Tolerance/ intolerance score**	**AFFECT PROTEIN FUNCTION (intolerance)**	**DOESN'T AFFECT PROTEIN FUNCTION (tolerance)**	**Seq Rep**
1.	T19I	0.10	no	yes	0.56
2.	G142D	0.18	no	yes	0.67
3.	K147E	0.86	no	yes	0.56
4.	W152R	0.17	no	yes	0.67
5.	F157L	0.75	no	yes	0.33
6.	I210V	1.00	no	yes	0.67
7.	V213G	0.25	no	yes	0.67
8.	G257S	0.85	no	yes	0.78
9.	G339H	0.16	no	yes	1.00
10.	R346T	0.34	no	yes	1.00
11.	S371F	0.26	no	yes	1.00
12.	S373P	0.38	no	yes	1.00
13.	S375F	**0.07**	no	yes	1.00
14.	T376A	0.33	no	yes	1.00
15.	D405N	0.27	no	yes	1.00
16.	R408S	0.87	no	yes	1.00
17.	K417N	0.56	no	yes	1.00
18.	N440K	0.70	no	yes	0.89
19.	G446S	0.79	no	yes	0.44
20.	N460K	1.00	no	yes	0.78
21.	S477N	0.84	no	yes	0.44
22	T478K	0.75	no	yes	0.44
23.	E484A	0.51	no	yes	0.56
24.	F486S	0.41	no	yes	0.44
25.	Q498R	0.39	no	yes	0.78
26.	N501Y	0.09	no	yes	0.89
27.	***Y505H***	***0.03***	***yes***	***no***	***0.89***
28.	D614G	0.62	no	yes	1.00
29.	H655Y	0.50	no	yes	0.78
30.	N679K	0.53	no	yes	0.67

31.	P681H	0.17	no	yes	0.56
32.	***N764K***	***0.00***	***yes***	***no***	***1.00***
33.	D796Y	1.00	no	yes	1.00
34.	Q954H	0.08	no	yes	1.00
35.	N969K	0.09	no	yes	1.00
36.	***D1199N***	***0.00***	***yes***	***no***	***1.00***

- ***Residues in italics and bold impairs protein function and caused an increased risk of disease.***

1. Threshold for intolerance is 0.05.
   1a. Less than 0.05 = intolerance = affects protein function.
   1b. More than 0.05 = tolerance = doesn't affects protein function.
2. **'Seq Rep'** is the fraction of sequences that contain one of the basic amino acids.
3. Threshold for intolerance is 0.05.
   3a. Less than 0.05 = intolerance = affects protein function.
   3b. More than 0.05 = tolerance = doesn't affects protein function.
4. **'Seq Rep'** is the fraction of sequences that contain one of the basic amino acids.

11.4.9. Salient structural features of RBD of spike protein (BA.2.75 and BA.2.75.2) when bound to ACE2 from MD simulation.

11.4.9.1. RMSD analysis.

To test the stability of the (S protein (BA.2.75)-ACE2) and (S protein (BA.2.75.2)-ACE2) complexes, 100 ns of MD simulation studies were carried out. The conformational snapshots of the (S protein (BA.2.75)-ACE2) and (S protein (BA.2.75.2)-ACE2) complexes during 100 ns MD simulation time were depicted in **Figure 7D.9 and Figure 7D.10**.

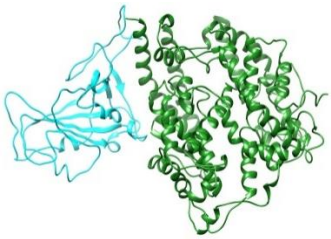
5 ns

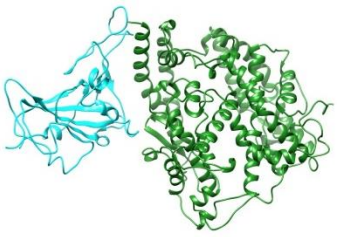
10 ns

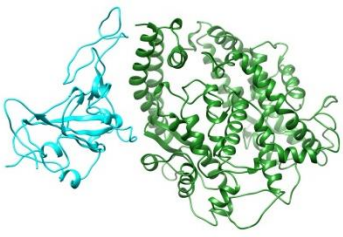
15 ns

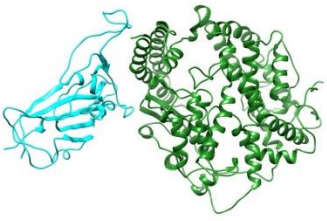
20 ns

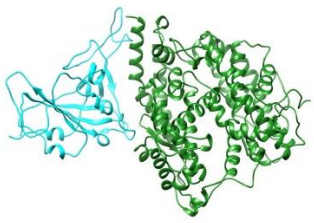
25 ns

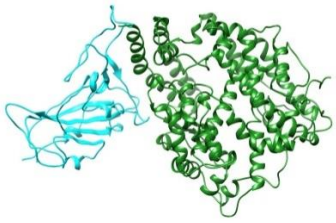
30 ns

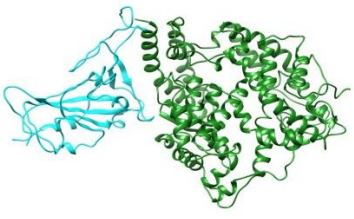
35 ns

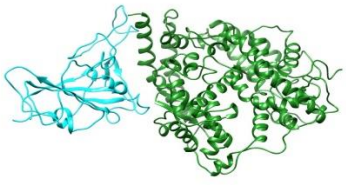
40 ns

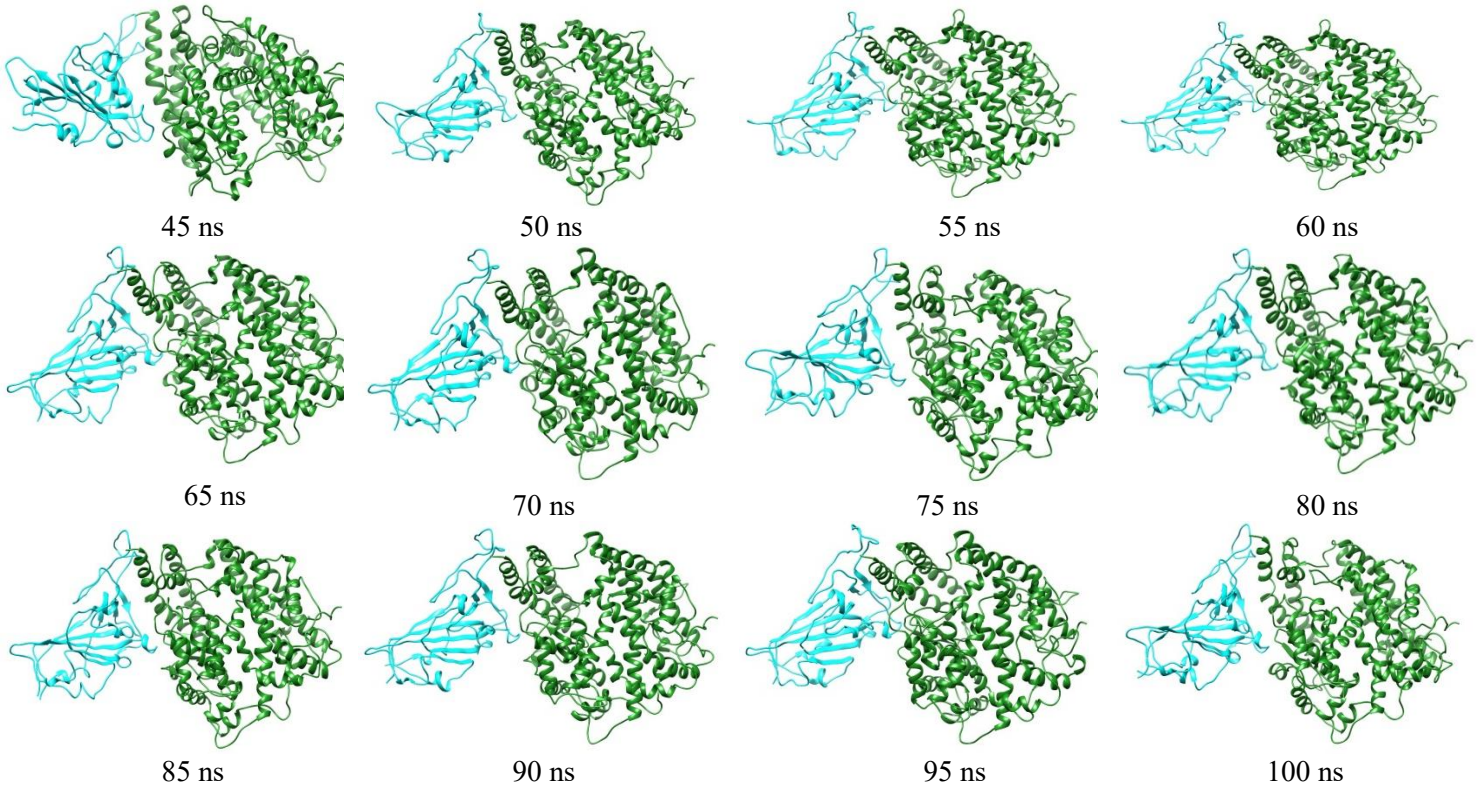

Figure 11.9. *Conformational snapshots of S protein (BA.2.75)-ACE2 complex at the time interval of 5 ns during the course of 100 ns of MD simulation.*

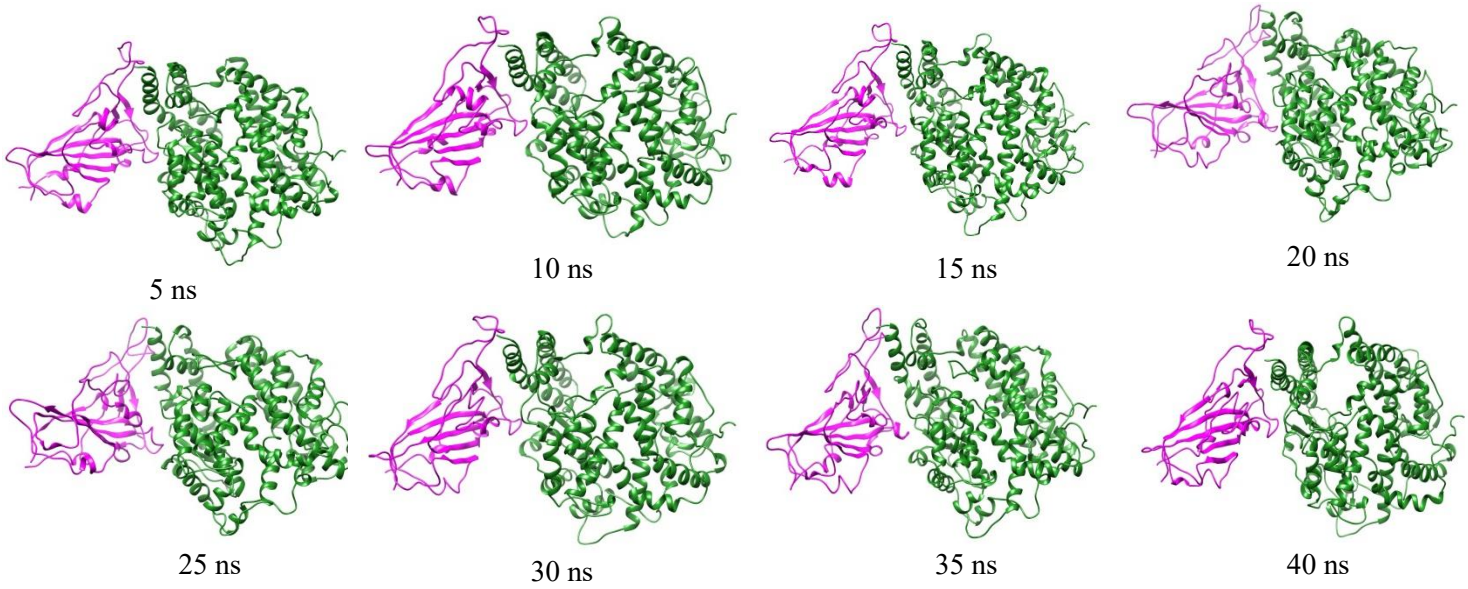

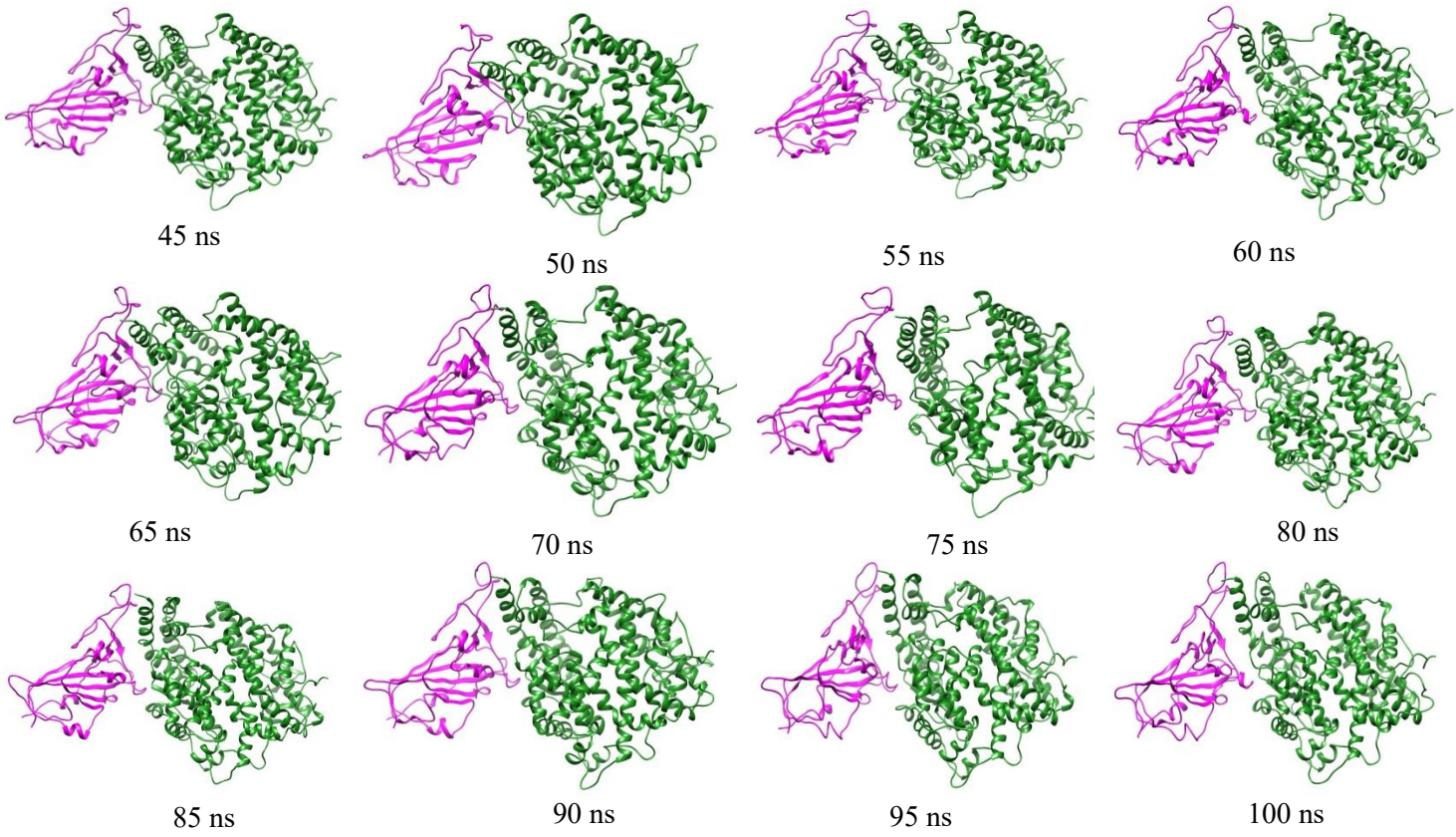

Figure 11.10. *Conformational snapshots of S protein (BA.2.75.2)-ACE2 complex at the time interval of 5 ns during the course of 100 ns of MD simulation.*

The average deviations in atomic locations and stability of the (S protein (BA.2.75)-ACE2) and (S protein (BA.2.75.2)-ACE2) complexes was depicted in **Figure 7D.11** and the stability of RBD of S protein in both the variants in the complex was compared and depicted in **Figure 7D.12.**

Interestingly, we noticed that the RMSD of the BA.2.75.2 complex was slightly higher than that of the BA.2.75 complex. The average RMSD value was found to be **2.4 Å (± 0.12)** for the BA.2.75 complex and **3.82 Å (± 0.14)** for the BA.2.75.2 complex. Hence it is apparent that S protein (BA.2.75)-ACE2 complex to be relatively more stable than the S protein (BA.2.75.2)-ACE2 complex.

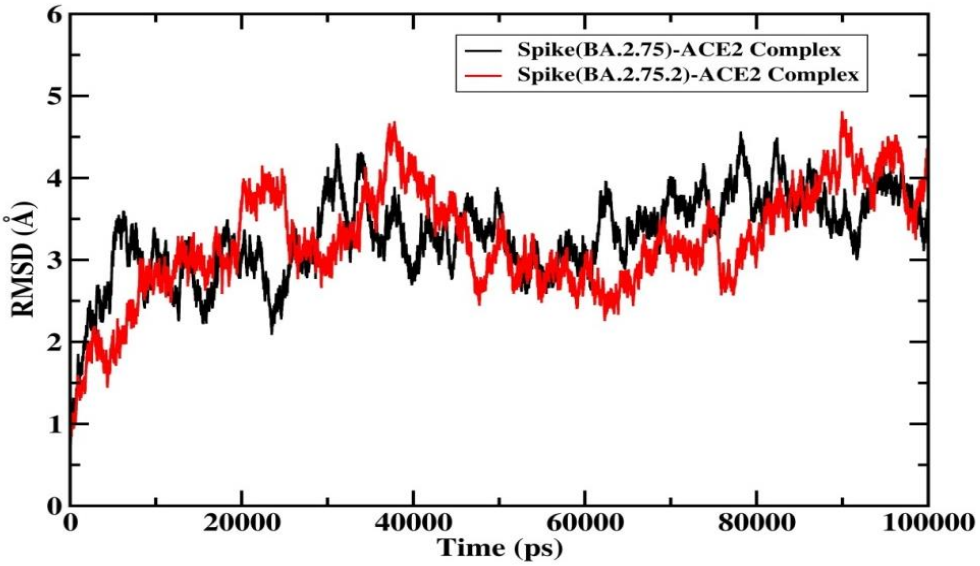

Figure 11.11. *Backbone RMSD's for S protein (BA.2.75)-ACE2 complex (black) and S protein (BA.2.75.2)-ACE2 complex (red)*

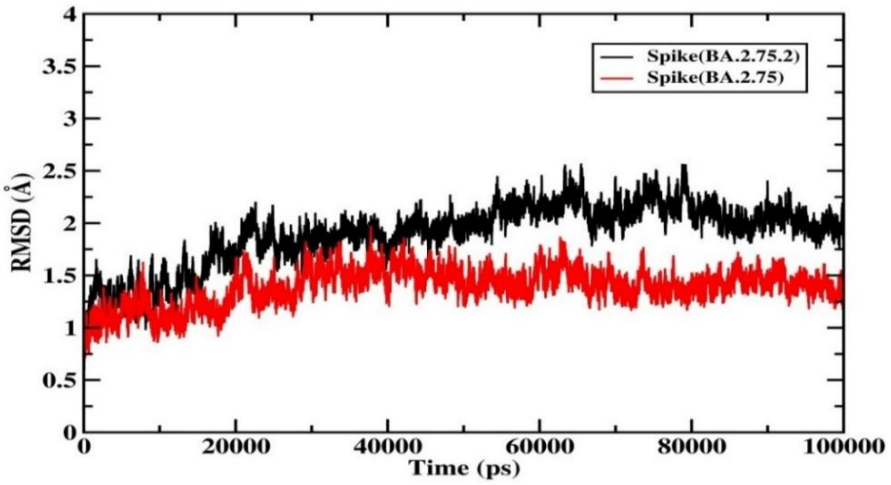

Figure 11.12. *Backbone RMSD's for S protein in S protein (BA.2.75.2)-ACE2 complex (black) and S protein (BA.2.75)-ACE2 complex (red)*

11.4.9.2. RMSF analysis.

We further explored the S protein flexibility in S protein (BA.2.75)-ACE2) and (S protein (BA.2.75.2)-ACE2) complexes by determining the Cα RMSF values from the MD simulations trajectory analysis. In **Figure 7D.13** the RMSF analysis of spike protein (BA.2.75 and BA.2.75.2) exclusively in the complex have been depicted while in **Figure 7D.14** the RMSF analysis for the entire complex have been shown.

We observed the structure of S protein in BA.2.75-ACE2 complex to have lesser fluctuations than in BA.2.75.2-ACE2 complex, hence inferring a greater stability to the S protein (BA.2.75.2)-ACE2 complex.

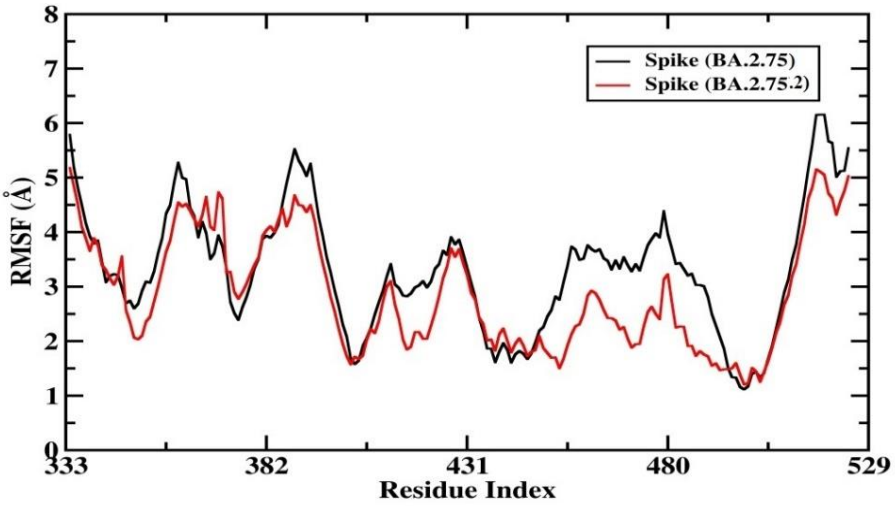

Figure 11.13. *Backbone RMSF's for S protein in S protein (BA.2.75)-ACE2 complex (black) and S protein (BA.2.75.2)-ACE2 complex (red).*

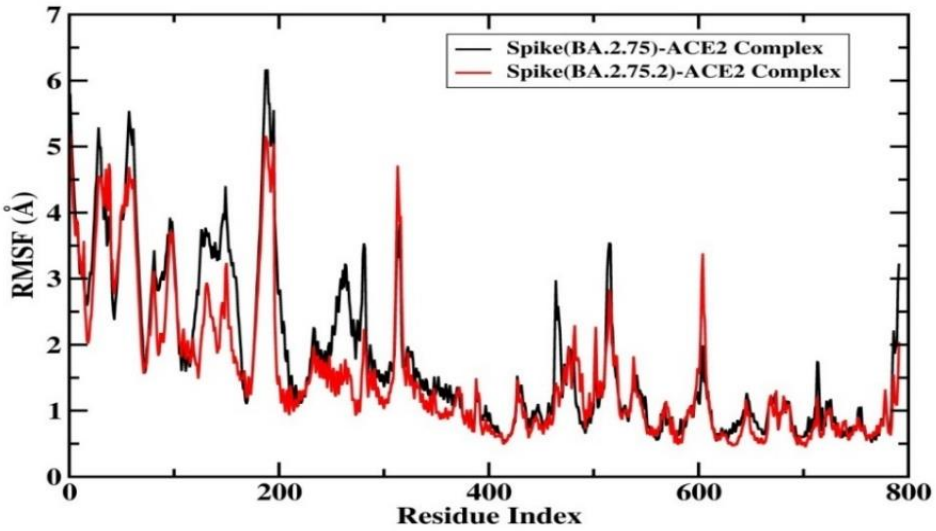

Figure 11.14. *Backbone RMSF's for S protein (BA.2.75)-ACE2 complex (Black) and S protein (BA.2.75.2)-ACE2 complex (Red).*

11.4.9.3. Hydrogen bond analysis.

The number of hydrogen bonds present was also calculated for the (S protein (BA.2.75)-ACE2) and (S protein (BA.2.75.2)-ACE2) complexes (**Figure 7D.15**), as these hydrogen bonds play a crucial role in

conferring stability to the protein complexes. The number of intermolecular hydrogen bonds was found to be higher in S protein (BA.2.75)-ACE2 complex than in S protein (BA.2.75.2)-ACE2 complex.

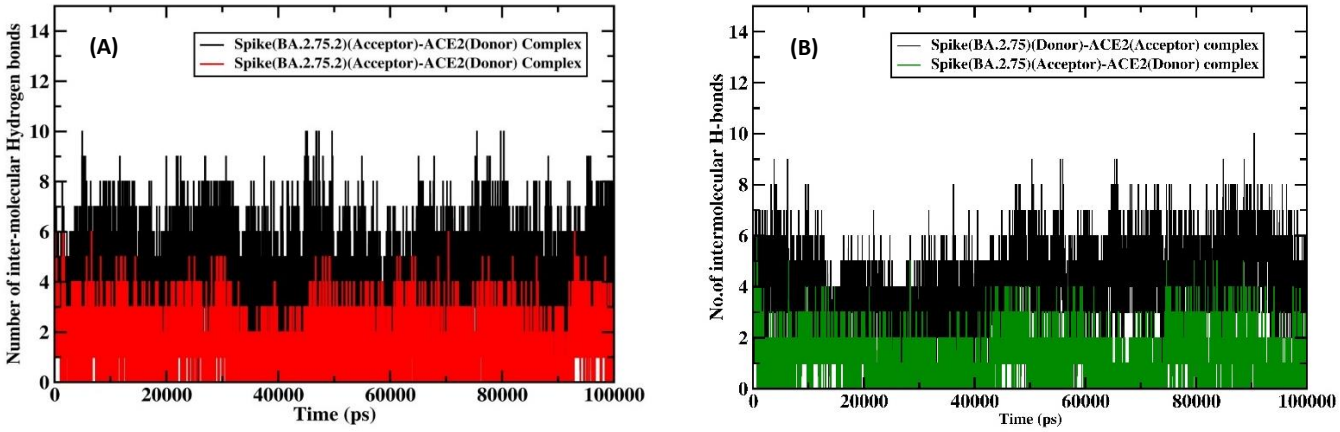

Figure. 11.15. *The number of intermolecular hydrogen bonds between S protein and ACE2 in* ***(A)*** *S protein (BA.2.75)-ACE2 complex and* ***(B)*** *S protein (BA.2.75.2)-ACE2 complex*

The list of intermolecular hydrogen bonds noticed between the S protein (BA.2.75/BA.2.75.2) (acceptor/donor) and ACE2(donor/acceptor) during the last 20 ns of MD simulation of both the complexes were summarized in **Table 11.15-11.18.**

Table 11.15: *Hydrogen bond analysis of S protein (BA.2.75)-ACE2 complex during the last 20 ns of MD simulation with S protein (BA.2.75) as acceptor and ACE2 as donor.*

#Acceptor	DonorH	Donor	Frac	Average Distance (Å)	Average Angles (°)
ALA_143@O	SER_196@HG	SER_196@OG	0.2364	2.7341	161.5817
GLN_161@OE1	LYS_208@HZ2	LYS_208@NZ	0.0969	2.7947	152.3155
GLN_161@OE1	LYS_208@HZ3	LYS_208@NZ	0.0919	2.796	152.1853
GLN_161@OE1	LYS_208@HZ1	LYS_208@NZ	0.0908	2.7916	151.4969
ALA_143@O	GLN_201@HE22	GLN_201@NE2	0.0839	2.8564	159.3664
GLY_170@HA3	GLY_531@HA3	GLY_531@CA	0.0446	2.9322	144.6
ASN_155@OD1	GLN_201@HE22	GLN_201@NE2	0.0426	2.8572	162.2502
ALA_143@O	SER_196@H1	SER_196@N	0.0415	2.8434	153.3316
ALA_143@O	SER_196@H2	SER_196@N	0.0335	2.8399	153.7224
HIE_173@ND1	LYS_530@HZ2	LYS_530@NZ	0.0327	2.9044	154.5345
THR_168@HG1	TYR_218@HH	TYR_218@OH	0.0311	2.8184	140.8474
ALA_143@O	SER_196@H3	SER_196@N	0.0255	2.8418	153.6045
HIE_173@ND1	LYS_530@HZ3	LYS_530@NZ	0.0253	2.9045	154.4186
THR_168@HG1	ARG_534@HH11	ARG_534@NH1	0.0222	2.8923	139.8468
HIE_173@ND1	LYS_530@HZ1	LYS_530@NZ	0.0198	2.9015	154.1666
HIE_173@HB3	LYS_530@HE3	LYS_530@CE	0.0141	2.9241	144.7558
PHE_124@HZ	LYS_208@HB2	LYS_208@CB	0.0119	2.9405	142.1763

GLN_161@HE21	LYS_208@HZ2	LYS_208@NZ	0.0108	2.8743	145.9434
ASN_155@HD21	GLN_201@HB3	GLN_201@CB	0.0065	2.8776	148.8844
GLY_170@H	GLY_531@HA3	GLY_531@CA	0.0059	2.87	139.9228
GLN_161@HE21	LYS_208@HZ1	LYS_208@NZ	0.0058	2.9018	147.458
GLN_161@HE21	LYS_208@HZ3	LYS_208@NZ	0.0056	2.914	146.2575
TYR_169@HE1	LYS_530@HE2	LYS_530@CE	0.0055	2.9246	143.6264
GLN_161@HE21	GLU_212@HB2	GLU_212@CB	0.005	2.888	143.2527

Table 11.16. *Hydrogen bond analysis of S protein (BA.2.75)-ACE2 complex during the last 20 ns of MD simulation with S protein (BA.2.75) as donor and ACE2 as acceptor*

#Acceptor	DonorH	Donor	Frac	Average Distance (Å)	Average Angles (°)
ASP_532@OD1	THR_168@HG1	THR_168@OG1	0.6923	2.7189	163.4831
LYS_530@O	GLY_170@H	GLY_170@N	0.6036	2.8757	164.5189
GLN_201@OE1	ASN_155@HD21	ASN_155@ND2	0.3972	2.8471	156.8261
GLU_212@OE2	GLN_161@HE21	GLN_161@NE2	0.3721	2.8248	163.1322
HIE_211@ND1	TYR_121@HH	TYR_121@OH	0.3375	2.8377	158.0876
ASP_215@OD2	TYR_169@HH	TYR_169@OH	0.3247	2.6991	158.0717
GLU_212@OE1	GLN_161@HE21	GLN_161@NE2	0.2732	2.8311	162.5669
TYR_218@OH	THR_168@HG1	THR_168@OG1	0.1893	2.8079	160.1612
TYR_218@HH	THR_168@HG1	THR_168@OG1	0.1703	2.8479	145.4137
ASP_215@OD1	TYR_169@HH	TYR_169@OH	0.0742	2.6904	158.9979
ASP_215@OD2	ARG_166@HH21	ARG_166@NH2	0.0521	2.8391	157.7429
TYR_260@OH	ASN_155@HD21	ASN_155@ND2	0.0502	2.8849	152.2469
ASP_215@OD1	ARG_166@HH21	ARG_166@NH2	0.0468	2.8023	152.0106
GLY_531@HA3	GLY_170@HA3	GLY_170@CA	0.0386	2.9262	140.9814
HIE_211@O	GLN_161@HE22	GLN_161@NE2	0.0366	2.8612	153.7524
TYR_260@HH	ASN_155@H	ASN_155@N	0.027	2.9135	152.6668
TYR_260@OH	ASN_155@H	ASN_155@N	0.0232	2.9194	154.2736
ASP_215@OD2	ARG_166@HE	ARG_166@NE	0.0184	2.901	156.3176
ARG_534@HH11	THR_168@HG1	THR_168@OG1	0.0168	2.8873	140.3772
GLN_502@OE1	GLN_174@HE21	GLN_174@NE2	0.0155	2.8665	164.1851
GLN_219@OE1	ARG_166@HH22	ARG_166@NH2	0.0148	2.8295	153.5704
LYS_208@HB2	PHE_124@HZ	PHE_124@CZ	0.0123	2.9492	141.9877
GLU_212@OE1	GLN_161@HE22	GLN_161@NE2	0.0095	2.8164	157.1018
GLN_201@HB3	ASN_155@HD21	ASN_155@ND2	0.008	2.8314	143.8366
LYS_530@HE3	HIE_173@HB3	HIE_173@CB	0.008	2.913	140.4817
GLN_219@OE1	ARG_166@HH12	ARG_166@NH1	0.0064	2.8331	153.3223
TYR_260@HE2	ASN_155@HD21	ASN_155@ND2	0.0062	2.8711	146.1065
TYR_260@HH	ASN_155@HD21	ASN_155@ND2	0.0055	2.9073	145.3465
GLN_201@HG2	ASN_155@HD21	ASN_155@ND2	0.0054	2.8427	145.3314

Table 11.17. *Hydrogen bond analysis of S protein (BA.2.75.2)-ACE2 complex during the last 20 ns of MD simulation with S protein (BA.2.75.2) as acceptor and ACE2 as donor.*

#Acceptor	DonorH	Donor	Frac	Average Distance (Å)	Average Angles (°)
ALA_143@O	SER_196@HG	SER_196@OG	0.2241	2.7344	161.3043
ASN_155@OD1	GLN_201@HE22	GLN_201@NE2	0.0861	2.8664	160.7953
GLY_170@HA3	GLY_531@HA3	GLY_531@CA	0.0674	2.925	142.0358
ALA_143@O	GLN_201@HE22	GLN_201@NE2	0.064	2.8571	159.1821
ASN_155@OD1	TYR_260@HH	TYR_260@OH	0.0636	2.7597	160.9757
THR_168@O	ASN_507@HD21	ASN_507@ND2	0.059	2.88	146.904
GLN_161@OE1	LYS_208@HZ2	LYS_208@NZ	0.0589	2.7929	155.8555
GLN_161@OE1	LYS_208@HZ3	LYS_208@NZ	0.0555	2.7974	154.4641
GLN_161@OE1	LYS_208@HZ1	LYS_208@NZ	0.0545	2.7934	154.9102
ASN_145@OD1	SER_196@H1	SER_196@N	0.0291	2.8193	153.233
ALA_143@O	SER_196@H2	SER_196@N	0.0252	2.8424	154.1039
TYR_163@O	LYS_530@HZ1	LYS_530@NZ	0.0248	2.816	146.4363
ALA_143@O	SER_196@H3	SER_196@N	0.0234	2.8421	153.7803
ALA_143@O	SER_196@H1	SER_196@N	0.0226	2.8342	153.6374
TYR_163@O	LYS_530@HZ3	LYS_530@NZ	0.0219	2.8215	146.4198
GLN_161@HE21	HIE_211@HB2	HIE_211@CB	0.0212	2.8679	155.1567
PHE_124@HZ	LYS_208@HB2	LYS_208@CB	0.0208	2.9505	142.35
ASN_145@OD1	SER_196@H3	SER_196@N	0.0196	2.8281	154.2356
TYR_163@O	LYS_530@HZ2	LYS_530@NZ	0.0196	2.8125	145.5505
ASN_145@OD1	SER_196@H2	SER_196@N	0.0168	2.8181	151.8784
THR_168@HA	ASN_507@HD21	ASN_507@ND2	0.0155	2.8858	148.9452
HIE_173@ND1	LYS_530@HZ3	LYS_530@NZ	0.0152	2.9045	148.9291
HIE_173@HB3	LYS_530@HE3	LYS_530@CE	0.0146	2.9203	143.3888
THR_168@HB	ASN_507@HD21	ASN_507@ND2	0.014	2.8141	144.969
HIE_173@ND1	LYS_530@HZ2	LYS_530@NZ	0.0123	2.9032	150.4128
THR_168@HG1	TYR_218@HH	TYR_218@OH	0.0103	2.8055	141.2792
HIE_173@ND1	LYS_530@HZ1	LYS_530@NZ	0.0096	2.9036	151.3484
PHE_158@O	LYS_208@HZ3	LYS_208@NZ	0.0081	2.8609	155.6833
GLY_170@H	GLY_531@HA3	GLY_531@CA	0.0063	2.8726	140.7923
ASN_145@OD1	SER_196@HG	SER_196@OG	0.0058	2.7503	162.4473
TYR_169@HE1	LYS_530@HE2	LYS_530@CE	0.0056	2.9333	142.7999
GLN_161@HE21	GLU_212@HB2	GLU_212@CB	0.0055	2.8865	143.2867
GLN_161@HE21	GLU_212@HG3	GLU_212@CG	0.0051	2.8389	146.5235

Table 11.18. *Hydrogen bond analysis of S protein (BA.2.75.2)-ACE2 complex during the last 20 ns of MD simulation with S protein (BA.2.75.2) as donor and ACE2 as acceptor.*

#Acceptor	DonorH	Donor	Frac	Average Distance (Å)	Average Angles (°)
LYS_530@O	GLY_170@H	GLY_170@N	0.5545	2.8842	163.4395
TYR_218@OH	THR_168@HG1	THR_168@OG1	0.5046	2.8213	159.5116
HIE_211@ND1	TYR_121@HH	TYR_121@OH	0.3802	2.8215	159.4365
ASP_215@OD2	TYR_117@HH	TYR_117@OH	0.3158	2.7166	161.4829
GLU_212@OE2	GLN_161@HE21	GLN_161@NE2	0.3002	2.8313	163.547
ASP_215@OD1	TYR_169@HH	TYR_169@OH	0.2806	2.6954	160.8994
ASP_532@OD1	THR_168@HG1	THR_168@OG1	0.2213	2.7202	163.5606
GLN_219@OE1	ARG_166@HH22	ARG_166@NH2	0.1564	2.8207	154.1051
GLN_201@OE1	ASN_155@HD21	ASN_155@ND2	0.1224	2.8573	156.4404
HIE_211@O	GLN_161@HE22	GLN_161@NE2	0.121	2.8594	157.4978
TYR_218@HH	THR_168@HG1	THR_168@OG1	0.1176	2.8817	147.4786
ASP_215@OD1	TYR_117@HH	TYR_117@OH	0.1144	2.7554	158.4637
GLU_212@OE1	GLN_161@HE21	GLN_161@NE2	0.1115	2.8299	163.1755
GLN_219@OE1	ARG_166@HH12	ARG_166@NH1	0.099	2.8293	153.3716
TYR_260@OH	ASN_155@HD21	ASN_155@ND2	0.0904	2.8928	152.514
GLN_502@OE1	GLN_174@HE21	GLN_174@NE2	0.0738	2.8601	162.9848
GLY_531@HA3	GLY_170@HA3	GLY_170@CA	0.0591	2.9234	141.2752
GLU_212@OE2	GLN_161@HE22	GLN_161@NE2	0.0345	2.823	157.1215
HIE_211@ND1	ARG_71@HH12	ARG_71@NH1	0.0343	2.9087	152.1668
ALA_564@O	ASN_73@HD21	ASN_73@ND2	0.0328	2.8862	155.6193
ASP_215@OD2	TYR_169@HH	TYR_169@OH	0.0293	2.6974	155.7449
GLN_201@OE1	ASN_145@H	ASN_145@N	0.0268	2.884	157.0237
HIE_211@HB2	GLN_161@HE21	GLN_161@NE2	0.0258	2.801	143.8054
GLU_212@OE1	GLN_161@HE22	GLN_161@NE2	0.0232	2.8306	157.3471
LYS_208@HB2	PHE_124@HZ	PHE_124@CZ	0.022	2.9463	142.4079
TYR_260@HH	ASN_155@HD21	ASN_155@ND2	0.0175	2.8999	147.2464
SER_196@O	ASN_145@HD21	ASN_145@ND2	0.0105	2.8783	156.4607
ASP_215@OD2	ARG_166@HH21	ARG_166@NH2	0.0092	2.8212	158.1953
LYS_530@HE3	HIE_173@HB3	HIE_173@CB	0.0082	2.9101	139.5733
ASN_507@HD21	THR_168@HB	THR_168@CB	0.0079	2.8404	142.7511
HIE_211@ND1	ARG_71@HH22	ARG_71@NH2	0.0078	2.9363	154.3691
GLU_212@HG3	GLN_161@HE21	GLN_161@NE2	0.0074	2.7983	146.0998
GLN_201@HG2	GLY_144@HA2	GLY_144@CA	0.0052	2.9361	144.3482

7D.4.9.4. Binding Free energy (BFE) and per residue energy decomposition (PRED) analysis.

Binding free energies of the S protein (BA.2.75)-ACE2 and S protein (BA.2.75.2)-ACE2 complexes were calculated from the last 10 ns of the MD simulation once the system reached equilibrium using MM-GBSA approach. The values here represent only the relative binding free energy rather than absolute or total binding energy, as MM-GBSA approach uses a continuum solvent approach to determine the binding free energies of a system. The binding free energies determined for the BA.2.75 and BA.2.75.2 complexes and the energy terms were summarized in **Tables 11.19 and 11.20**. From Table 7D.19 and 7D.20, it can be seen that S protein (BA.2.75)-ACE2 complex (GB_{TOT} = -20.03 kcal/mol, was energetically more favorable than the S protein (BA.2.75.2)-ACE2 complex (GB_{TOT} = -15.1959 kcal/ mol). Tables 7D.16 and 7D.17 show that all BFE components contributed to S protein and ACE2 binding to form the S protein (BA.2.75/BA.2.75.2)-ACE2 complex.

Table 11.19. *Binding free energies (kcal/mol) and its components of S protein (B.A.2.75)-ACE2 complex obtained using MM-GBSA approach.*

	$\Delta G_{(S\ protein(BA.2.75)-ACE2)} - [\Delta G_{S\ protein(BA2.75)} + \Delta G_{ACE2}]$ (kcal/mol)	
	Average	**std. dev. (±)**
VDW	-86.96	3.75
ELE	-1497.14	24.00
GB	1576.30	24.71
GBSUR	-12.23	0.30
GAS	-1584.11	24.51
GBSOL	1564.07	24.58
GBTOT	**-20.03**	4.41

Table 11.20. *Binding free energies (kcal/mol) and its components of S protein (B.A.2.75.2)-ACE2 complex obtained using MM-GBSA approach.*

	$\Delta G_{(S\ protein(BA.2.75.2)-ACE2)} - [\Delta G_{S\ protein(BA2.75.2)} + \Delta G_{ACE2}]$ (kcal/mol)	
	Average	**std. dev. (±)**
VDW	-88.37	3.10
ELE	-1228.04	22.32
GB	1302.26	21.48
GBSUR	-12.54	0.31
GAS	-1296.41	22.02
GBSOL	1292.71	21.50
GBTOT	**-15.19**	3.98

PRED values were also calculated for gaining insights into the contribution of each amino acid residue to the overall protein-protein interaction. In this analysis, the total binding energy was decomposed into residues to identify key residues for ACE2 binding to S protein (BA.2.75/BA.2.75.2). Essential residues with the binding energy value below -1.00 kcal/mol are shown in **Figures 7D.16 and 7D.17**. The residues that contribute the highest energy for S protein in BA.2.75 complex is TYR 501, PHE 486, GLN 493, HIE 505, PHE 456, LEU 455, TYR 489, THR 500, ALA 475, GLY 502 while in S protein (BA.2.75.2) comes from the residues TYR 501, HIE 505, PHE 456, TYR 489, LEU 455, THR 500, GLN 493, ALA 475, GLY 502, TYR 453.

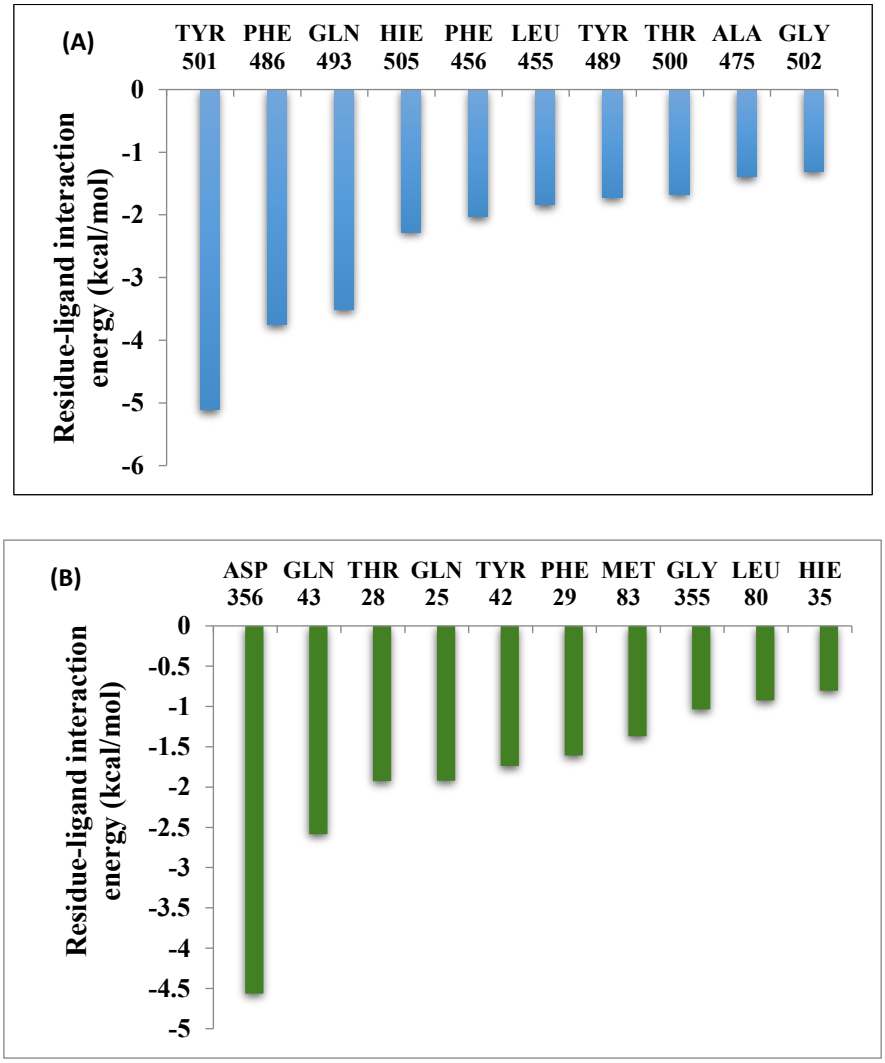

Figure 11.16. *Decomposition of binding free energy (kcal/mol) on per residue basis for ACE2 binding to S protein (BA.2.75) obtained using MM-GBSA approach for* ***(A)*** *Spike (BA.2.75)* ***(B)*** *ACE2.*

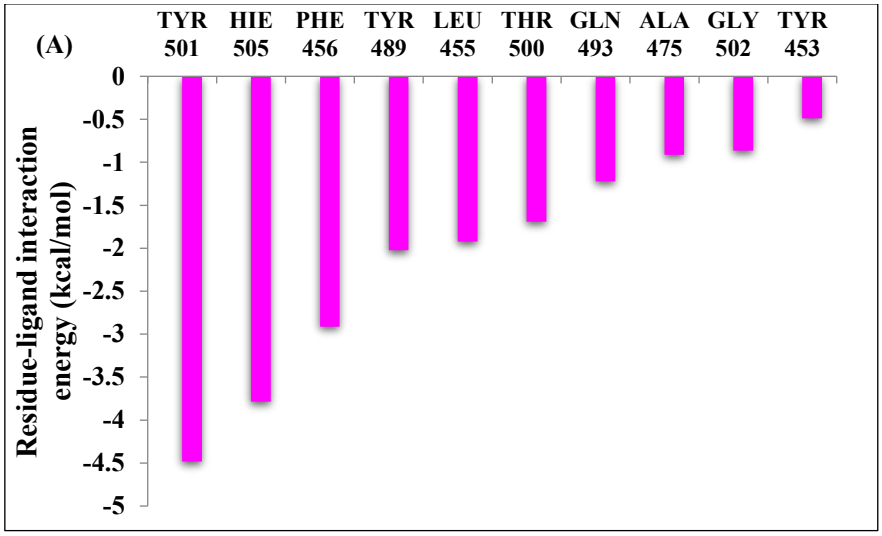

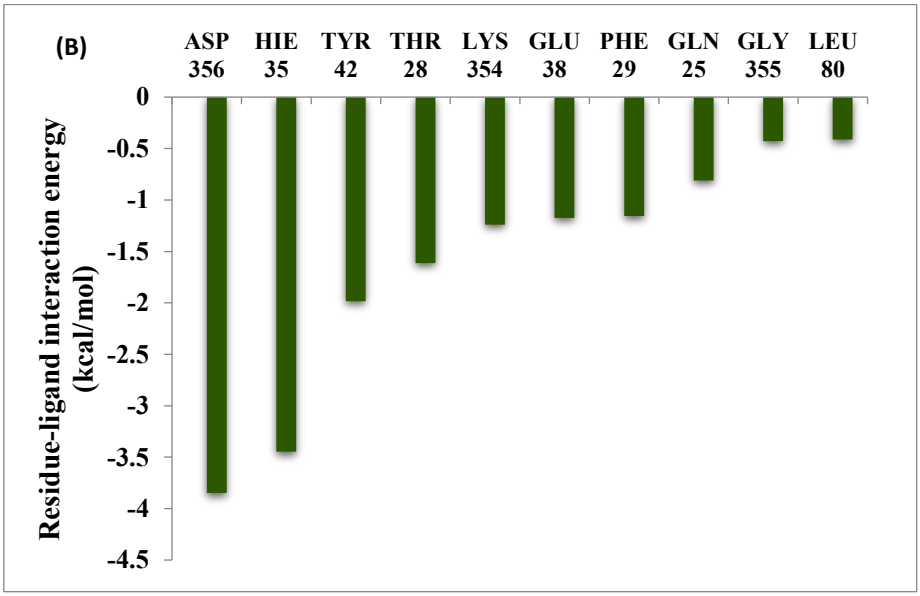

Figure 11.17. *Decomposition of binding free energy (kcal/mol) on per residue basis for ACE2 binding to S protein (BA.2.75.2) obtained using MM-GBSA approach for* ***(A)*** *Spike (BA.2.75.2)* ***(B)*** *ACE2.*

Discussion: Molecular dynamics and in-silico analyses performed here shows that the BA.2.75 complex is more stable and interactive than BA.2.75.2, supported by lower RMSD/RMSF values, a larger interface and more hydrogen bonds and non-bonded contacts. Binding free energy calculations and per-residue contributions from key residues like Tyr501, Phe486, and Gln493 further confirm stronger affinity in BA.2.75. These findings not only explain the

potentially higher transmissibility of BA.2.75 but also identify conserved energetic hotspots that could guide the design of effective broad-spectrum inhibitors targeting spike–ACE2 interactions.

11.5. Conclusion:

Key physiochemical characteristics, structural characteristics, and binding characteristics of BA.2.75 and BA.2.75 omicron variants were examined using computational methods. The physio-chemical characteristics revealed that both omicron variants were stable over a wide temperature range. These variants were found to exhibit secondary structural characteristics that were more or less comparable, with the secondary structure alpha helix dominating, followed by an extended strand and random coil. The BA.2.75 and BA.2.75.2 sequences had a considerably larger proportion of identity (similarity) in their sequence, followed by the Wuhan-Hu-1 and BA.2.75 and Wuhan-Hu-1 and BA.2.75.2 sequences. These variants followed a similar trend from the intrinsically disordered region prediction and were found to contain 84 disordered residues and 10 disordered regions with a 6.61 disordered percentage. It was determined from the analysis of protein stability after mutation that the mutations N501Y and H655Y make these variants more stable. From the protein-protein interaction study, we observed the total number of interactions (Hydrogen bonds and non-bonded) to be higher in the case of the spike (BA.2.75)-ACE2 complex in comparison with spike (BA2.75.2)-ACE2 complex. From the SIFT analysis, we found that for the BA.2.75 variant, Y505H and N764K impaired protein function and an increased risk of disease whereas in BA.2.75.2, the three mutations Y505H, N764K and D1199N were observed to impair the protein function.

This present study also demonstrates the effect of BA.2.75 and BA.2.75.2 variants on SARS-CoV-2 RBD towards its binding with the ACE2 by employing MD simulation and other computational approaches. From the RMSD, RMSF, and number of inter-molecular hydrogen bond analyses, we found the S protein (BA.2.75)-ACE2 complex to have enhanced stability than the S protein (BA.2.75.2)-ACE2 complex. The number of non-bonded contacts is also higher in the S protein (BA.2.75)-ACE2 complex. From the binding free energy calculations of the S protein (BA.2.75)-ACE2 and S protein (BA.2.75.2)-ACE2 complexes, we found that the BA.2.75 Spike-ACE2 complex's affinity between S protein and ACE2 is higher. The overall stability of the S protein (BA.2.75)-ACE2 complex and the increased affinity between S protein (BA.2.75) and ACE2 may result in higher virulence of the strain.

11.6. Bibliography:

[1]. Han, H.J., Nwagwu, C., Anyim, O., Ekweremadu, C., and Kim, S. COVID-19 and cancer: From basic mechanisms to vaccine development using nanotechnology. *International Immunopharmacology*, 90, 107247, 2021. http://doi.org/10.1016/j.intimp.2020.107247

[2]. Sheward, D.J., Kim, C., Fischbach, J., Muschiol, S., Ehling, R.A., Björkström, N.K., Hedestam, G. B.K., Reddy, S.T., Albert, J., Peacock, T.P., and Murrell, B. Evasion of neutralising antibodies by omicron sublineage BA.2.75. *The Lancet Infectious Diseases*, 22(11): 1421–1422, 2022. http://doi.org/10.1016/s1473-3099(22)00524-2

[3]. Kumar, S. Protein-Protein Interaction Network for the Identification of New Targets Against Novel Coronavirus. In Silico Modeling of Drugs Against Coronaviruses. *Methods in Pharmacology and Toxicology*, edited by K. Roy, Humana, New York, NY, 213-230, 2021. http://doi.org/10.1007/7653_2020_62

[4]. Scarpa, F., Sanna, D., Azzena, I., Giovanetti, M., Benvenuto, D., Angeletti, S., Ceccarelli, G., Pascarella, S., Casu, M., Fiori, P.L., and Ciccozzi, M. On the SARS-CoV-2 BA.2.75 variant: A genetic and structural point of view. *Journal of Medical Virology*, 95(1): e28119, 2022. http://doi.org/10.1002/jmv.28119

[5]. Yamasoba, D., Kosugi, Y., Kimura, I., Fujita, S., Uriu, K., Ito, J., and Sato, K. Genotype to Phenotype Japan (G2P-Japan) Consortium. Neutralization sensitivity of SARS-COV-2 omicron subvariants to therapeutic monoclonal antibodies. *The Lancet Infectious Diseases*, 22(7): 942–943, 2022. http://doi.org/10.1016/s1473-3099(22)00365

[6]. Verma, J., and Subbarao, N. Structural Insight into Antibody Evasion of SARS-Cov-2 Omicron Variant. *Virology and Immunology Journal*, 6: 000289, 2022. http://doi.org/10.23880/vij-16000289

[7]. Zhou, H., Tada, T., D'Costa, B.M., and Landau, N.R. Neutralization of SARS-COV-2 Omicron BA.2 by Therapeutic Monoclonal Antibodies. *bioRxiv*, 2022. http://doi.org/10.1101/2022.02.15.480166.

[8]. Kim, J., Seo, H., Kim, H.W., Kim, D., Kwon, H.J., and Kim, Y.K. Effect of Previous COVID-19 Vaccination on Humoral Immunity 3 Months after SARS-CoV-2 Omicron Infection and Booster Effect of a Fourth COVID-19 Vaccination 2 Months after SARS-CoV-2 Omicron Infection. *Viruses*, 14(11): 2458, 2022. http://doi.org/10.3390/v14112458

[9]. Shaheen, N., Mohamed, A., Soliman, Y., Abdelwahab, O.A., Diab, R.A., Desouki, M.T., Rababah, A.A., Khaity, A., Hefnawy, M.T., Swed, S., Shaheen, A., Elfakharany, B., and Shoib, S. Could the new BA.2.75 subvariant lead to another COVID-19 wave in the world? *International Journal of Surgery*, 105: 106861, 2022. http://doi.org/10.1016/j.ijsu.2022.106861

[10]. Dai, Y. Rapid epidemic expansion of the SARS-COV-2 Omicron BA.2 subvariant during China's

largest outbreaks. *Research Square*, 2022. http://doi.org/10.21203/rs.3.rs-1516063/v6

[11]. Iacobucci G. Covid-19: Runny nose, headache, and fatigue are commonest symptoms of omicron, early data show. *BMJ (Clinical research ed.)*, 375: n3103, 2021. https://doi.org/10.1136/bmj.n3103

[12]. Shrestha, L.B., Foster, C., Rawlinson, W., Tedla, N., and Bull, R.A. Evolution of the SARS-CoV-2 omicron variants BA.1 to BA.5: Implications for immune escape and transmission. *Reviews in Medical Virology*, 32 (5): e2381, 2022. http://doi.org/10.1002/rmv.2381

[13]. Harvey, W.T., Carabelli, A.M., Jackson, B., Gupta, R.K., Thomson, E.C., Harrison, E.M., Ludden, C., Reeve, R., Rambaut, A., COVID-19 Genomics UK (COG-UK) Consortium, Peacock, S.J., and Robertson, D.L. SARS CoV-2 variants, spike mutations and immune escape. *Nature Reviews Microbiology*, 19(7): 409–424, 2021. https://doi.org/10.1038/s41579-021-00573-0

[14]. Peng, R., Wu, L.A., Wang, Q., Qi, J., and Gao, G.F. Cell entry by SARS-CoV-2. *Trends in Biochemical Sciences*, 46(10):848–860, 2021. https://doi.org/10.1016/j.tibs.2021.06.001

[15]. Pathania, A.S., Prathipati, P., Abdul, B.A.A., Chava, S., Katta, S.S., Gupta, S.C., Gangula, P.R., Pandey, M.K., Durden, D.L., Byrareddy, S.N., and Challagundla, K.B. COVID-19 and Cancer Comorbidity: Therapeutic Opportunities and Challenges. *Theranostics*, 11(2):731–753, 2021. https://doi.org/10.7150/thno.51471

[16]. Mongia, A., Saha, S.K., Chouzenoux, E., and Majumdar, A. A computational approach to aid clinicians in selecting anti-viral drugs for COVID-19 trials. *Scientific Reports*, 11, 9047, 2021. https://doi.org/10.1038/s41598-021 88153-3

[17]. Behera, S.K., Vhora, N., Contractor, D., Shard, A., Kumar, D., Kalia, K., and Jain, A. Computational drug repurposing study elucidating simultaneous inhibition of entry and replication of novel corona virus by Grazoprevir. *Scientific Reports*, 11(1): 7307, 2021. https://doi.org/10.1038/s41598-021-86712-2

[18]. Egieyeh, S., Egieyeh, E., Malan, S., Christoffels, A., and Fielding, B. Computational drug repurposing strategy predicted peptide-based drugs that can potentially inhibit the interaction of SARS-CoV-2 spike protein with its target (human ACE2). *PLOS ONE*, 16, e0245258, 2021. https://doi.org/10.1371/journal.pone.0245258

[19]. Coban, M.A., Morrison, J., Maharjan, S., Hernandez Medina, D.H., Li, W., Zhang, Y.S., Freeman, W.D., Radisky, E.S., Le Roch, K.G., Weisend, C.M., Ebihara, H., and Caulfield, T.R. Attacking COVID-19 Progression Using Multi-Drug Therapy for Synergetic Target Engagement. *Biomolecules*, 11(6):787, 2021. http://doi.org/10.3390/biom11060787

[20]. Basak, S.C., and Kier, L.B. COVID-19 Pandemic: How can Computer-assisted Methods help to Rein in this Global Menace? *Current Computer-Aided Drug Design*, 17(1):1, 2021. http://doi.org/10.2174/1573409917012101121032l5

[21]. Ibrahim, M.A.A., Abdelrahman, A.H.M., Allemailem, K.S., Almatroudi, A., Moustafa, M.F., and

Hegazy, M.E.F. In Silico Evaluation of Prospective Anti-COVID-19 Drug Candidates as Potential SARS-CoV-2 Main Protease Inhibitors. *The Protein Journal*, 40(3): 296–309, 2021. https://doi.org/10.1007/s10930-020-09945-6

[22]. Singh, S.K., Upadhyay, A.K., and Reddy, M.S. Screening of potent drug inhibitors against SARS-CoV-2 RNA polymerase: an in-silico approach. *Biotech*, 11(2):93, 2021. http://doi.org/10.1007/s13205-020-02610-w

[23]. Enmozhi, S.K., Raja, K., Sebastine, I., and Joseph, J. Andrographolide as a potential inhibitor of SARS-CoV-2 main protease: an in-silico approach. *Journal of Biomolecular Structure and Dynamics*, 39(9): 3092–3098, 2021. http://doi.org/10.1080/07391102.2020.1760136

[24]. Verma, J., and Subbarao, N. In silico study on the effect of SARS-CoV-2 RBD hotspot "mutants" interaction with ACE2 to understand the binding affinity and stability. *Virology*, 561, 107–116, 2021. https://doi.org/10.1016/j.virol.2021.06.009

[25]. Teruel, N., Mailhot, O., and Najmanovich, R.J. Modeling conformational state dynamics and its role on infection for SARS-CoV-2 Spike protein variants. *PLOS Computational Biology*, 17 (8): e1009286, 2021. https://doi.org/10.1371/journal.pcbi.1009286

[26]. Noh, J.Y., Jeong, H.W., and Shin, E.C. SARS-CoV-2 mutations, vaccines, and immunity: implication of variants of concern. *Signal Transduction and Targeted Therapy*, 6(1):203, 2021. https://doi.org/10.1038/s41392-021-00623-2

[27]. Abdellatiif, M.H., Ali, A., Ali, A., and Hussien, M.A. Computational studies by molecular docking of some antiviral drugs with COVID-19 receptors as an approach to medication for COVID-19. *Open Chemistry*, 19(1):245–264, 2021. https://doi.org/10.1515/chem-2021-0024

[28]. Abebe, E.C., Dejenie, T.A., Shiferaw, M.Y., and Malik, T. The newly emerged COVID-19 disease: a systematic review. *Virology Journal*, 17(1):96, 2020. http://doi.org/10.1186/s12985-020-01363-5

[29]. Leung, N.H.L. Transmissibility and transmission of respiratory viruses. *Nature Reviews Microbiology*, 19(8):528–545, 2021. http://doi.org/10.1038/s41579-021-00535-6

[30]. Kumar, S., Mathavan, S., Jin, W.J., Bt-Azman, N.A., Subramaniam, D., Zainalabidin, N.A.B., Lingadaran, D., Sattar, Z.B.A., Manickam, D.L., Anbananthan, P.S., Taqiyuddin, J.A., and Thevarajan, Y. COVID-19 vaccine candidates by identification of B and T cell multi-epitopes against SARS-COV-2. *Preprints*, 2020080092, 2020. https://doi.org/10.20944/preprints202008.0092.v1

[31]. Kumar, S., Thambiraja, T.S., Karuppanan, K., and Subramaniam, G. Omicron and Delta variant of SARS-CoV-2: A comparative computational study of spike protein. *Journal of Medical Virology*, 94(4):1641–1649, 2021. http://doi.org/10.1002/jmv.27526

[32]. Kumar, S. Drug and vaccine design against novel coronavirus (2019-nCoV) spike protein through computational approach. *Preprints*, 2020020071, 2020. https://doi.org/10.20944/preprints202002.0071.v1.

[33]. Pandey, S.C., Pande, V., Sati, D., Upreti, S., and Samant, M. Vaccination strategies to combat novel coronavirus SARS-CoV-2. *Life Sciences*, 256, 117956, 2020. http://doi.org/10.1016/j.lfs.2020.117956

[34]. Gasteiger, E., Gattiker, A., Hoogland, C., Ivanyi, I., Appel, R.D., and Bairoch, A. ExPASy: The proteomics server for in-depth protein knowledge and analysis. *Nucleic Acids Research*, 31(13): 3784-3788, 2003. https://doi.org/10.1093/nar/gkg563

[35]. Sen, T.Z., Jernigan, R.L., Garnier, J., and Kloczkowski, A. GOR V server for protein secondary structure prediction. *Bioinformatics*, 21(11): 2787-2788, 2005. https://doi.org/10.1093/bioinformatics/bti408

[36]. Sievers, F., and Higgins, D.G. Clustal Omega, accurate alignment of very large numbers of sequences. In Multiple Sequence Alignment Methods; Russell, D. (Ed.); *Methods in Molecular Biology*, Vol. 1079, Humana Press: Totowa, NJ, 105-116, 2013. https://doi.org/10.1007/978-1-62703-646-7_6

[37]. Xue, B., Dunbrack, R.L., Williams, R.W., Dunker, A.K., and Uversky, V.N. PONDR-FIT: A meta-predictor of intrinsically disordered amino acids. *Biochimica et Biophysica Acta - Proteins and Proteomics*, 1804(4): 996-1010, 2010. https://doi.org/10.1016/j.bbapap.2010.01.011

[38]. Capriotti, E., Fariselli, P., and Casadio, R. I-Mutant2.0: predicting stability changes upon mutation from the protein sequence or structure. *Nucleic Acids Research*, 33, W306-W310, 2005. https://doi.org/10.1093/nar/gki375

[39]. Berman, H.M., Westbrook, J., Feng, Z., Gilliland, G., Bhat, T.N., Weissig, H., Shindyalov, I.N., and Bourne, P.E. The Protein Data Bank. *Nucleic Acids Research*, 28(1):235-242, 2000. https://doi.org/10.1093/nar/28.1.235.

[40]. Pettersen, E.F., Goddard, T.D., Huang, C.C., Couch, G.S., Greenblatt, D.M., Meng, E.C., and Ferrin, T.E. UCSF Chimera—A visualization system for exploratory research and analysis. *Journal of Computational Chemistry*, 25(13):1605-1612, 2004. http://doi.org/10.1002/jcc.20084.

[41]. Laskowski, R.A., Hutchinson, E.G., Michie, A.D., Wallace, A.C., Jones, M.L., and Thornton, J.M. PDBsum: a web-based database of summaries and analyses of all PDB structures. *Trends in Biochemical Sciences*, 22 (12):488-490, 1997. https://doi.org/10.1016/s0968-0004(97)01140-7

[42]. Ng, P.C., and Henikoff, S. SIFT: predicting amino acid changes that affect protein function. *Nucleic Acids Research*, 31(13):3812-3814, 2003. https://doi.org/10.1093/nar/gkg509

[43]. Case, D.A., Cheatham III, T.E., Darden, T., Gohlke, H., Luo, R., Merz Jr., K.M., Onufriev, A., Simmerling, C., Wang, B., and Woods, R.J. The Amber biomolecular simulation programs. *Journal of Computational Chemistry*, 26(16): 1668-1688, 2005. https://doi.org/10.1002/jcc.20290

[44]. Maier, J.A., Martinez, C., Kasavajhala, K., Wickstrom, L., Hauser, K.E., and Simmerling, C. ff14SB: Improving the accuracy of protein side chain and backbone parameters from ff99SB. *Journal of Chemical Theory and Computation*, 11(8):3696-3713, 2015. https://doi.org/10.1021/acs.jctc.5b00255

[45]. Jorgensen, W.L., Chandrasekhar, J., Madura, J.D., Impey, R.W., and Klein, M.L. Comparison of simple potential functions for simulating liquid water. *Journal of Chemical Physics*, 79, 926-935, 1983. https://doi.org/10.1063/1.445869

[46]. Yoo, S., and Xantheas, S.S. Communication: The effect of dispersion corrections on the melting temperature of liquid water. *Journal of Chemical Physics*, 134(12):121105, 2011. https://doi.org/10.1063/1.3573375

[47]. Darden, T., York, D., and Pedersen, L. Particle mesh Ewald: An N·log(N) method for Ewald sums in large systems. *Journal of Chemical Physics*, 98(12):10089-10092, 1993. https://doi.org/10.1063/1.464397

[48]. Salomon-Ferrer, R., Götz, A.W., Poole, D., Le Grand, S., and Walker, R.C. Routine microsecond molecular dynamics simulations with AMBER on GPUs. 2. Explicit solvent particle mesh Ewald. *Journal of Chemical Theory and Computation*, 9 (9):3878-3888, 2013. https://doi.org/10.1021/ct400314y

[49]. Kräutler, V., van Gunsteren, WF., and Hünenberger, P.H. A fast SHAKE: Algorithm to solve distance constraint equations for small molecules in molecular dynamics simulations. *Journal of Computational Chemistry*, 22(5):501-508, 2001. https://doi.org/10.1002/1096-987x(20010415)22:53.0.co;2-v

[50]. Berendsen, H.J.C., Postma, J.P.M., van Gunsteren, W.F., DiNola, A., and Haak, J.R. Molecular dynamics with coupling to an external bath. *Journal of Computational Physics*, 81, 3684-3690, 1984. https://doi.org/10.1063/1.448118

[51]. Chen, F., Liu, H., Sun, H., Pan, P., Li, Y., Li, D., and Hou, T. Assessing the performance of the MM/PBSA and MM/GBSA methods. Capability to predict protein-protein binding free energies and re-rank binding poses generated by protein-protein docking. *Physical Chemistry Chemical Physics*, 18, 22129-22139, 2016. https://doi.org/10.1039/C6CP03670H

[52]. Genheden, S., and Ryde, U. The MM/PBSA and MM/GBSA methods to estimate ligand-binding affinities. *Expert Opinion on Drug Discovery*, 10 (5): 449-461, 2015. http://doi.org/10.1517/17460441.2015.1032936

[53]. Sun, H., Duan, L., Chen, F., Liu, H., Wang, Z., Pan, P., Zhu, F., Zhang, J.Z.H., and Hou, T. Assessing the performance of MM/PBSA and MM/GBSA methods. 7. Entropy effects on the performance of end-point binding free energy calculation approaches. *Physical Chemistry Chemical Physics*, 20, 14450-14460, 2018. https://doi.org/10.1039/c7cp07623a

[54]. Wang, E., Sun, H., Wang, J., Wang, Z., Liu, H., Zhang, J.Z.H., and Hou, T. End-point binding free energy calculation with MM/PBSA and MM/GBSA: Strategies and applications in drug design. *Chemical Reviews*, 119(16): 9478-9508, 2019. https://doi.org/10.1021/acs.chemrev.9b00055

[55]. Das, C., Das, D., and Mattaparthi, V.S.K. Effect of mutations in the SARS-CoV-2 spike RBD

region of Delta and Delta-plus variants on its interaction with ACE2 receptor protein. *Letters in Applied NanoBioScience*, 12, 118, 2023. https://doi.org/10.33263/LIANBS124.118

[56]. Das, C., Das, D., and Mattaparthi, V.S.K. Computational investigation on the efficiency of small molecule inhibitors identified from Indian spices against SARS-CoV-2 Mpro. *Biointerface Research in Applied Chemistry*, 13 (2):235, 2023. https://doi.org/10.33263/BRIAC133.235

[57]. Das, C., and Mattaparthi, V.S.K. Impact of mutations in the SARS-CoV-2 spike RBD region of BA.1 and BA.2 variants on its interaction with ACE2 receptor protein. *Biointerface Research in Applied Chemistry*, 13(4):358, 2023. https://doi.org/10.33263/BRIAC134.358

[58]. Das, C., Hazarika, P.J., Deb, A., Joshi, P., Das, D., and Mattaparthi, V.S.K. Effect of double mutation (L452R and E484Q) in RBD of spike protein on its interaction with ACE2 receptor protein. *Biointerface Research in Applied Chemistry*, 13, 97, 2022. https://doi.org/10.33263/BRIAC131.097